Systems/Circuits

Paraventricular Thalamic *MC3R* Circuits Link Energy Homeostasis with Anxiety-Related Behavior

Dajin Cho,[1,2*] Kyle O'Berry,[1,2*] Ingrid Camila Possa-Paranhos,[1] Jared Butts,[1,2] Naraen Palanikumar,[1] and Patrick Sweeney[1,2]

[1]Department of Molecular and Integrative Physiology, University of Illinois Urbana-Champaign, Urbana, Illinois 61801 and [2]Neuroscience Program, University of Illinois Urbana-Champaign, Urbana, Illinois 61801

The hypothalamic melanocortin system is critically involved in sensing stored energy and communicating this information throughout the brain, including to brain regions controlling motivation and emotion. This system consists of first-order agouti-related peptide (AgRP) and pro-opiomelanocortin (POMC) neurons located in the hypothalamic arcuate nucleus and downstream neurons containing the melanocortin-3 (*MC3R*) and melanocortin-4 receptor (*MC4R*). Although extensive work has characterized the function of downstream *MC4R* neurons, the identity and function of *MC3R*-containing neurons are poorly understood. Here, we used neuroanatomical and circuit manipulation approaches in mice to identify a novel pathway linking hypothalamic melanocortin neurons to melanocortin-3 receptor neurons located in the paraventricular thalamus (PVT) in male and female mice. *MC3R* neurons in PVT are innervated by hypothalamic AgRP and POMC neurons and are activated by anorexigenic and aversive stimuli. Consistently, chemogenetic activation of PVT *MC3R* neurons increases anxiety-related behavior and reduces feeding in hungry mice, whereas inhibition of PVT *MC3R* neurons reduces anxiety-related behavior. These studies position PVT *MC3R* neurons as important cellular substrates linking energy status with neural circuitry regulating anxiety-related behavior and represent a promising potential target for diseases at the intersection of metabolism and anxiety-related behavior such as anorexia nervosa.

Key words: **anxiety; feeding behavior; *MC3R*; melanocortins; paraventricular thalamus**

Significance Statement

Animals must constantly adapt their behavior to changing internal and external challenges, and impairments in appropriately responding to these challenges are a hallmark of many neuropsychiatric disorders. Here, we demonstrate that paraventricular thalamic neurons containing the melanocortin-3 receptor respond to energy-state-related information and external challenges to regulate anxiety-related behavior in mice. Thus, these neurons represent a potential target for understanding the neurobiology of disorders at the intersection of metabolism and psychiatry such as anorexia nervosa.

Introduction

Animals must constantly adapt their behavior to changing internal (i.e., hunger/satiety) and environmental challenges (i.e., threats in the environment), and select the appropriate behavioral response to underlying needs. For example, although increased behavioral approach and food seeking is necessary to prevent starvation in hungry animals, the same behavior is not adaptive in sated animals as this may result in exposure to predators or injury (Burnett et al., 2016, 2019; Sutton and Krashes, 2020). Inappropriate behavioral responses to internal and external challenges commonly occur in multiple neuropsychiatric disorders, such as anorexia nervosa (AN), anxiety disorders, and mood disorders. In the case of AN, patients do not appropriately seek and consume food despite severe hunger as the psychosocial stress and stigma associated with food consumption presumably override the homeostatic drive to eat (Keski-Rahkonen et al., 2007; Herpertz-Dahlmann et al., 2012). Thus, it is of critical importance to understand the downstream neural circuitry mediating behavioral responses to hunger, particularly given the lack of effective therapeutics for neuropsychiatric eating disorders (Hay et al., 2012).

The central melanocortin system consists of agouti-related protein (AgRP) and pro-opiomelanocortin (POMC) neurons in the hypothalamic arcuate nucleus, which sense stored energy in

Received Apr. 19, 2023; revised Aug. 3, 2023; accepted Aug. 8, 2023.

Author contributions: P.S. designed research; D.C., K.O., I.C.P., J.B., and P.S. performed research; N.P. contributed unpublished reagents/analytic tools; D.C., K.O., I.C.P., N.P., and P.S. analyzed data; and D.C., K.O., and P.S. wrote the paper.

This work was supported by National Institutes of Health–National Institute of Diabetes and Digestive and Kidney Diseases Grant R00DK127065 (P.S.), the Foundation for Prader Willi Research (P.S.), and Brain and Behavior Research Foundation Grant 100000874 (P.S.).

*D.C. and K.O. contributed equally to this work.

P.S. owns stock in Courage Therapeutics. All the other authors declare no competing financial interests.

Correspondence should be addressed to Patrick Sweeney at sweenp@illinois.edu.

https://doi.org/10.1523/JNEUROSCI.0704-23.2023

the form of leptin from fat, gut-derived satiety hormones and glucose levels in the blood (Cone, 2005; Garfield et al., 2009). AgRP neurons are activated during hunger (Takahashi and Cone, 2005), resulting in the release of the melanocortin receptor antagonist AgRP at downstream brain regions containing melanocortin receptor 3 or 4 (Cone, 2005, 2006). Conversely, POMC neurons are activated in the satiated state (Cowley et al., 2001; Chen et al., 2015; Mandelblat-Cerf et al., 2015) or in response to stress (Liu et al., 2007; Qu et al., 2020), resulting in the release of the melanocortin receptor agonist alpha-melanocyte stimulating hormone (aMSH). Further, AgRP and POMC neurons are rapidly modulated by the sight of food and/or by cues predicting food availability (Betley et al., 2015; Chen et al., 2015; Mandelblat-Cerf et al., 2015; Beutler et al., 2017; Su et al., 2017), indicating that these neurons sense both current physiological state and predicted outcomes to adaptively control behavior. Chemogenetic and optogenetic activation of AgRP and POMC neurons produces opposing effects on feeding and behavior, with AgRP neuron stimulation increasing feeding (Aponte et al., 2011; Krashes et al., 2011, 2013) and reducing anxiety-related behavior (Dietrich et al., 2015; Burnett et al., 2016, 2019; Padilla et al., 2016; Li et al., 2019), and POMC neuron stimulation reducing feeding (Zhan et al., 2013) and increasing anxiety-related behavior (Lee et al., 2020; Qu et al., 2020; Fang et al., 2021). Thus, POMC and AgRP neurons sense the energy state of the animal and environmental conditions predicting food availability in real time and communicate this information to downstream melanocortin-receptor-expressing neurons to initiate an appropriate behavioral response to hunger or satiety. However, the cell types and neural circuits mediating downstream behavioral responses to hunger and satiety are incompletely understood.

An extensive literature has characterized the critical role of *MC4R* in mediating the anorexic effects of melanocortins (Cone, 2005; Krashes et al., 2016) as global deletion of *MC4R* leads to hyperphagic obesity in both rodents (Huszar et al., 1997) and humans (Farooqi et al., 2000; Vaisse et al., 2000; Farooqi et al., 2003). AgRP and POMC neurons project to *MC4R*-containing neurons in the paraventricular hypothalamus (PVN) where aMSH activates *MC4R* to reduce feeding, while AgRP inhibits *MC4R* to increase feeding (Fenselau et al., 2017; Ghamari-Langroudi et al., 2015; Cone, 2005; Sweeney et al., 2021a; Shah et al., 2014). In contrast to *MC4R*, *MC3R* knock-out mice exhibit a complicated metabolic and endocrine phenotype characterized by minor late-onset obesity, defective fast-induced refeeding, increased anxiety, delayed puberty and growth, and an enhanced response to anorexic stimuli (Butler et al., 2000; Sweeney et al., 2021b; Ghamari-Langroudi et al., 2018; Lam et al., 2021). Although *MC3R* is expressed throughout the brain, the specific function of *MC3R* is unknown in most *MC3R*-containing sites (Bedenbaugh et al., 2022).

One candidate *MC3R*-containing site for mediating downstream behavioral effects of AgRP and POMC neurons is the paraventricular thalamic nucleus (PVT). AgRP and POMC neurons project densely throughout the PVT (Betley et al., 2013; Wang et al., 2015), and activation of AgRP projections to the PVT increases feeding (Betley et al., 2013) while also prioritizing attention and cognition toward smells and cues associated with food versus nonfood objects (Livneh et al., 2017; Horio and Liberles, 2021). Prior studies support an important role for PVT circuits in regulating motivation (Labouèbe et al., 2016; Campus et al., 2019; Choi et al., 2019; Otis et al., 2019; Hill-Bowen et al., 2020; McNally, 2021), anxiety (Kirouac, 2015, 2021; Penzo et al., 2015; Choi and McNally, 2017; Levine et al., 2021), and aversive behavior (Kirouac, 2015; Penzo et al., 2015; Zhu et al., 2016; Levine et al., 2021) and for balancing reward seeking with threat avoidance (Kirouac, 2015; Choi and McNally, 2017; Choi et al., 2019; Hill-Bowen et al., 2020; McNally, 2021; Penzo and Gao, 2021). Thus, the PVT is a critical neural structure mediating adaptive behavioral responses to underlying needs and environmental conditions (Choi and McNally, 2017; Choi et al., 2019; Meffre et al., 2019; Otis et al., 2019; Hill-Bowen et al., 2020; McGinty and Otis, 2020; McNally, 2021). However, although previous work has established the importance of hypothalamic-derived peptides (i.e., orexin) in regulating anxiety-related behavior in PVT (Li et al., 2010a, b; Heydendael et al., 2011; Meffre et al., 2019), the specific cell types in PVT linking energy homeostasis to anxiety-related behavior are unknown. Here, we use a combination of circuit manipulation approaches, neuroanatomy, molecular genetics, and *in vivo* imaging to characterize a novel role of PVT *MC3R* neurons in controlling anxiety-related behavior.

Materials and Methods

Animals

All animal experiments were approved by the University of Illinois Institutional Animal Care and Use Committee. All experiments were performed on littermate mice that were approximately matched for age and body weight between experimental and control groups. Experiments were performed on an approximate equal amount of male and female mice (depending on the number of each sex generated during breeding). For illustrating main effects of manipulations, data from both sexes are collapsed in the main text figures, and any interactions between sex and outcome variables are also illustrated in main text figures. Transgenic mouse lines included *MC4R-Cre* (catalog #030759, The Jackson Laboratory), *MC3R-Cre* (Ghamari-Langroudi et al., 2018), *MC3R floxed*, and tdtomato floxed (catalog #007914, The Jackson Laboratory). Transgenic *MC3R-Cre*, *MC4R-Cre*, and *MC3R-Flox* mice were genotyped by submitting ear samples to Transnetyx to confirm the presence of Cre and Flox alleles, respectively. Tdtomato mice were bred as homozygous mice and crossed to either *MC3R-Cre* or *MC4R-Cre* heterozygous mice to generate either *MC4R-Cre*; *tdtomato* or *MC3R-Cre*; tdtomato transgenic lines. Both *MC4R-Cre* (Garfield et al., 2015) and *MC3R-Cre* mice (Ghamari-Langroudi et al., 2018; Sweeney et al., 2021b) have been previously published, and Cre expression was verified to faithfully label *MC4R-* or *MC3R*-containing cells (Bedenbaugh et al., 2022), respectively.

MC3R floxed mice were generated by Taconic using CRISPR-Cas9 gene editing approaches. Guide RNA to the *MC3R* gene, donor vector containing loxP sites, and Cas9 mRNA were coinjected into fertilized mouse eggs to generate targeted conditional knock-out offspring. Filial (F)0 founder animals were identified by PCR followed by sequence analysis and were bred to wild-type mice to test germline transmission and F1 animal generation. *MC3R floxed* mice were bred as heterozygote × heterozygote to generate littermate flox/flox and WT mice for experiments.

Before social isolation, all mice were caged in groups of two to five of the same sex. Mice were housed in temperature-controlled (19–21°C) and humidity-controlled cages. The room was under a 12 h light/dark cycle with the light period beginning at 6:00 A.M. and the dark cycle beginning at 6:00 P.M. All mice had *ad libitum* access to regular chow and water, unless otherwise noted in the text and figure legends. During experiments that required fasting, the mice were fasted overnight from 4:00 P.M. to 10:00 A.M.

Viral vectors

Adeno-associated virus (AAV) vectors used included Cre-dependent Gcamp8m (AAV1-syn-FLEX-jGCamp8m), Cre-dependent hM3Dq (AAV5-syn-DIO-hM3D-mCherry), Cre-dependent hM4Di (AAV5-hsyn-DIO-hM4D-mCherry), Cre-dependent control virus (AAV5-syn-

DIO-mcherry), Cre-dependent Kir 2.1 (AAV-EF1a-DIO-Kir2.1-P2A-dTomato), and Cre-expressing virus (AAV9-hSyn-HI.eGFP Cre). All viral vectors were purchased from Addgene, with the exception of Kir2.1 which was a gift from Benjamin Arenkiel (Baylor University).

Stereotaxic viral injections. In advance to stereotaxic surgery, mice went through anesthesia inside an isoflurane chamber and were positioned in a stereotaxic frame (Kopf) with a constant flow of isoflurane. A dental drill was used to drill a hole on top of the viral injection site, and the dura was removed. The AAV viral vectors were injected into the paraventricular thalamus (PVT) using a micromanipulator (Narishige) attached to a pulled glass pipette with a pipette holder (Ronal Tool). Viral injection coordinates for the PVT were as follows: AP, −0.75 mm and −1.40 mm (from the bregma); ML, 0.0 mm; DV, −3.00 mm, −2.85 mm, and −2.75 mm (from surface of the brain). In each AP coordinate, three injections of viral vectors were delivered in three DV coordinates, and 75 nl of virus was injected in each DV site at a rate of 50 nl/min. After the injection, the glass pipette was left in place for an additional 5 min to prevent leaking of virus from the targeted brain region. For fiber photometry experiments, GCamp8m was injected into PVT using the same injection coordinates and volumes described above. In the same surgery, a 200 um fiber optic fiber (0.66 NA, Plexon) was implanted directly into PVT with the coordinates as follows (AP, −1.20; ML, 0.0; DV, −2.70). Fiber optic cannula were secured to the skull using dental cement (C&B Metabond). Silicone sealant (Kwik-Cast) was used to fill the incision site. Mice were returned to their home cages and went through a recovery period of at least 2 weeks for viral expression and recovery from surgery before the experiments. After the injections, 3 d of carprofen injection was administered subcutaneously (5 mg/kg) to reduce pain.

Perfusion, sectioning, and immunohistochemistry

Following experiments all virally injected mice were perfused with 10% formalin followed by removal of brain tissue. Brains were transferred to a 10% formalin solution for 24 h for further fixation, followed by 24 h of increasing amounts of sucrose concentration (10, 20, and 30%). Brain slices containing PVT were then obtained by sectioning on a Leica (CM3050 S) cryostat at a 40 μm thickness. These sections were then placed into 24 well plates containing 500 μl of blocking buffer (100 ml 1× PBS, 2 g bovine serum albumin, and 100 μl of Tween 20) and placed on a shaker at room temperature and allowed to sit for 2 h. Next, a master mix of the following relevant antibodies: c-*fos* (9F6 rabbit mAb, 1:1000; Cell Signaling Technology), rabbit AgRP (1:1000; catalog #H-003-57, Phoenix Pharmaceuticals), rabbit POMC (1:1000; catalog #H-029-30, Phoenix Pharmaceuticals) in blocking buffer was prepared. Then 500 μl of this master mix was added to each well containing brain sections and placed onto a shaker in a cold room (4°C) and incubated for 24 h. The primary antibody mixture was then removed and replaced with 500 μl of ultra-pure 1× PBS and placed on a shaker at room temperature for 10 min. The PBS was then replaced with fresh ultra-pure PBS and placed back on the shaker for another 10 min with the process repeated one more time. A 1:500 concentration of secondary antibodies [goat Anti-Rabbit IgG (H + L) Cross-Adsorbed Secondary Antibody, Alexa Fluor 488] was prepared in blocking buffer. After removing the ultra-pure PBS from the well plate, 500 μl of the 1:500 secondary was added to each well and placed on a shaker at room temperature and incubated for an additional 2 h. Following three 10 min wash steps with 1× ultra-pure PBS, the sections were mounted on Superfrost glass slides (Thermo Fisher Scientific) and imaged with confocal microscopy (Zeiss LSM 510).

c-fos *Quantification and analysis*

For c-*fos* quantification, tissue was prepared as described above. Injections of CNO (0.3 mg/kg, i.p., 200 μl saline; Enzo Life Sciences) or saline (0.9% NaCL, 200 μl, i.p.) were performed 1 h before perfusion to confirm designer receptor exclusively activated by designer drugs (DREADD) mediating activation of PVT *MC3R* neurons. For fed versus refed analysis, mice were fasted overnight and allowed to refeed for 1 h before perfusion, whereas fed *ad libitum* mice were perfused at the same time of day but were not fasted. For setmelanotide experiments, setmelanotide (1 mg/kg, i.p., 200 ul saline; catalog #A20689, AdooQ Bioscience) or saline (200 ul, i.p.) was injected 1 h before perfusion, and mice were returned to their home cage after intraperitoneal injections with food and water *ad libitum*. This time point was chosen (1 h poststimulus) because we previously demonstrated robust c-*fos* labeling in other cell types expressing hM3Dq DREADD between 30 min to 1 h after CNO injections (Ghamari-Langroudi et al., 2018; Sweeney and Yang, 2015). For each experiment, the overlap between PVT *MC3R* neurons and c-*fos* was performed using ImageJ software. The total number of PVT *MC3R* cells was first counted (labeled with mCherry), and the percentage of these cells coexpressing with c-*fos* was quantified. For each mouse, we counted overlap from at least three to five representative PVT sections, and an average percentage of overlap was calculated for each mouse from these representative sections for statistical comparison.

RNAscope in situ *hybridization and mRNA quantification*

RNAscope analysis was performed on C57BL/6J mice. Mice were perfused as described above, and 20 um sections were directly mounted onto Superfrost glass slides for RNAscope *in situ* hybridization. RNAscope multiplex fluorescent *in situ* hybridization version 2 protocol was followed according to the protocol described in the kit using the Mm-Mc3r-C2 probes (catalog #412541-C2), Mm-Slc17a6 (catalog #319171), and Mm-Slc32a1 (catalog #319191), and images were obtained via confocal microscopy. The mRNA count was performed using Fiji/ImageJ software, where a region of interest (ROI) was created and placed on the area with high mRNA (Advanced Cell Diagnostics, catalog # 323100) expression in the PVT region. The mRNA was manually counted, and the same ROI size was used for all the images.

Behavioral experiments

Feeding behavior assays. For feeding experiments, mice were single housed for at least 1 week before testing, with the exception of social-isolation-induced anorexia assays (see below). A premeasured amount of food was placed in the food hopper, and the mice were changed to a new cage daily. Food intake was measured at ascending time points by weighing the food in the hopper and subtracting from the original food weight. For chemogenetic experiments injections of CNO (0.3 mg/kg, 200 ul in saline, i.p.) or saline (200 ul, i.p.) were administered 15 min before testing.

Social isolation anorexia. Social isolation anorexia experiments were performed as previously described (Sweeney et al., 2021b; Possa-Paranhos et al., 2023). Briefly, mice were single caged, and food intake was measured 1 h later. On the next day, food intake was measured again at the same time of day, and the difference in food intake on the social isolation day was compared with the following day. For experiments with chemogenetic inhibition, CNO (0.3 mg/kg) was administered 15 min before social isolation.

Open field test. Before beginning open field experiments mice were allowed 30 min to acclimate to the new environment of the behavioral testing room. An open field box (40 × 40 cm), was placed underneath a behavioral tracking camera connected to a Plexon system for tracking mouse movement (Plexon CineLyzer). Mice had not been exposed previously to the open field, and thus this represented a novel experience. The center area of the open field was added to the Plexon system to automatically register when the mice were in the center area of the open field. Mice were then placed in the corner of the open field, and the Plexon system began recording their movement. Mice were allowed to explore the open field for 5 min before being removed. The open field was then cleaned with 70% alcohol before another mouse was added. For experiments involving the injection of CNO, mice were injected 15 min before their entry into the open field. The Plexon system recorded time spent in the center, entries to the center, total distance traveled, and tracked movement in space.

Elevated zero maze. Before the start of the elevated zero maze test (EZM; MazeEngineers) mice were allowed 30 min to acclimate to the new environment of the behavioral testing room. The elevated zero maze consists of a raised circular platform that has two high-walled

sections along the circular walkway as well as two no-walled sections. The section of the maze with high walls is considered the closed arms area and is designated as such in the Plexon software. The area with no walls is considered the open-arms area and is again designated as such in the Plexon software. At the start of the test, mice are placed into one of the closed-arms areas and allowed to move freely around the maze for 5 min. During this time the behavioral camera and tracking system monitored the entries of the mice into the open arms, time in open arms, as well as distance traveled and speed. For experiments requiring intraperitoneal injection of CNO, mice were injected 15 min before their entry into the maze. The maze was cleaned with 70% alcohol between each mouse.

Novelty suppressed feeding test. The day before novelty suppressed feeding (NSF) testing, food was removed from the cages, and the mice were placed into fresh cages without food at 4:00 P.M. The following morning mice were brought to the behavioral room at 9:30 A.M. and allowed 30 min to acclimate to the new environment. The same box used for the open field test (OFT) was used for the NSF test, but there was a period of 1 week between the tests to allow for the environment of the box to remain novel. The arena of the box was mapped alongside a center arena where the food pellet was placed. The test began by first placing a new food pellet in the center arena and then placing a mouse in one of the corners of the arena. The mouse was then allowed to explore the environment and consume the food pellet for 10 min. After 10 min the mouse was removed from the arena, and the arena was then cleaned with 70% alcohol before placing a new mouse and pellet in the arena. For experiments requiring intraperitoneal injection of CNO, mice were injected 15 min before their entry into the arena. Latency to consume food was measured after testing for each mouse by visually inspecting NSF videos after testing. Eating was counted when the mouse chewed on the food pellet for at least 5 s.

Order of behavioral and feeding experiments

Following surgical intervention mice were allowed 2 weeks to recover and allow for viral expression. During this period mice were group caged with two to five mice per cage and remained this way until feeding studies were performed. For all cohorts, mice were run through behavioral experiments (i.e., EZM, OFT) while group caged before feeding experiments were performed. The only exception to this was a single cohort of *MC3R*-Flox mice where social isolation was performed before the beginning of behavioral experiments. Subsequent cohorts of *MC3R*-Flox mice that had behavioral experiments while group caged showed statistically similar results to the cohort that was single caged before behavioral tests. and as such these cohorts were combined for statistical analysis. Open field tests were performed first followed 1–2 d later by the EZM. Social isolation and feeding experiments followed 3–5 d after the completion of behavioral experiments.

Fiber photometry behavioral studies

Following surgery for GCamp expression and fiber optic placement, mice were allowed 2 weeks to recover and for expression of the GCamp protein. This was followed by a 3–5 d acclimation period. During this period mice were brought into the behavioral room and had an optical patch cable attached and then were allowed to walk freely around their cages for 10 min. Fiber photometry experiments were performed using a Plexon multiwavelength photometry system.

In the water presentation task mice were attached to the fiber optic patch cord, and the calcium signal was recorded for 2 min in the mouse home cage. Following 2 min of baseline recording, mice were introduced to a small piece of Kimwipes soaked in water (5 ml) and placed in a small Petri dish at the corner of the cage. The Petri dish was covered with a lid to prevent the mice from directly contacting the Kimwipe. Changes in signal were recorded for an additional 5 min following the presentation of water. For each mouse the average *Z*-scored signal and the maximum *Z*-scored signal was calculated in both the baseline 2 min period and the 5 min period following water exposure. The difference between these two signals (after water minus before water) was calculated for the 5 min following water exposure for each mouse for statistical comparison.

For EZM experiments mice were allowed to explore the elevated zero maze for 5 min while recording calcium activity. Plexon video tracking software automatically scored the time that the mice spent in the open arms versus closed arms during 5 min in the EZM. Calculated times were independently scored manually to confirm the computers calculations. Time in the open arms and time in the closed arms were aligned to the fiber photometry software and the *Z*-scored average and *Z*-scored maximum signal was compared for each mouse during the time in the open arms and the time in the closed arms. The difference in this signal (open arms minus closed arms) was calculated for each mouse for statistical comparison.

To record calcium signal changes in response to trimethylthiazoline (TMT) exposure, experiments were performed identically as described for water exposure except that mice were exposed to a Kimwipe containing TMT (5 ml). For acute restraint experiments calcium signal was recorded for 1 min for a baseline recording. Mice were then manually restrained by the experimenter by grabbing the mouse and preventing movement for 10 s. Following this 10 s restraint period, mice were released from restraint and calcium signal was recording for an additional 1 min. The mean and maximum *Z*-scored calcium signal was calculated for the 1 min baseline period (prerestraint) and for the 10 s restraint period. The change in mean and maximum *Z*-scored calcium signal was computed for each mouse by subtracting the baseline signal (prerestraint) from the signal during restraint.

Fiber photometry analysis

Fiber photometry numerical and graphical results were tabulated through custom code written in R software using the rshiny package to display a graphical interface. The interface accepts data input via two file selection bars that each accept a CSV file. The first selection bar accepts raw photometry data, and the second accepts event-related data. The raw photometry data CSV file is formatted with three relevant columns that come directly from the Plexon fiber photometry system. These columns include a times tamp, raw 410 nm fluorescence data (isobestic control channel for potential nonspecific effects of motion), and raw 465 nm fluorescence data (GCAMP signal). Through this format of CSV, baseline (410 nm) and signal data (465 nm) are encoded for each time point throughout an experiment and can be manipulated within the program. The second CSV file for events is composed of three relevant columns, an event description (i.e., entering the open arm), an event starting time, and an event ending time. These event segments are superimposed on the fluorescence data. To calculate the *Z*-score normalized photometry data we first subtracted the control channel (410 nm) from the signal channel (465 nm) and then divided by the control channel. The resultant baseline normalized values were then scaled so that measurements are represented in SDs from a mean. All plots were rendered using the ggplot2 and plotly packages in R. Changes in signal during behavioral experiments were calculated by comparing the average and maximum *Z*-score of fluorescence during the event versus before the event for water exposure, restraint, and TMT presentation. For EZM tests the mean and maximum *Z*-score of fluorescent activity was compared during periods where the mice were in the open arms versus periods when they were in the closed arms, and the difference between the open arms and closed arms signals was calculated for each mouse (open arm signal minus closed arm signal).

Data analysis and statistics

All mice with viral injections were perfused and sectioned following experiments. Only animals with viral targeting localized to the PVT were included in analysis. Normality tests were performed on all data to determine whether data followed a normal distribution. Normally distributed data were analyzed with parametric tests, whereas data without a normal distribution were analyzed with nonparametric tests. Specific statistical tests are further outlined in the figure legends. Data were analyzed using GraphPad software.

Results

PVT *MC3R* neurons are anatomically positioned between hypothalamic melanocortin neurons and subcortical anxiety circuitry

Hypothalamic AgRP and POMC neurons project throughout the brain to secondary sites containing the *MC3R* and *MC4R* (Betley

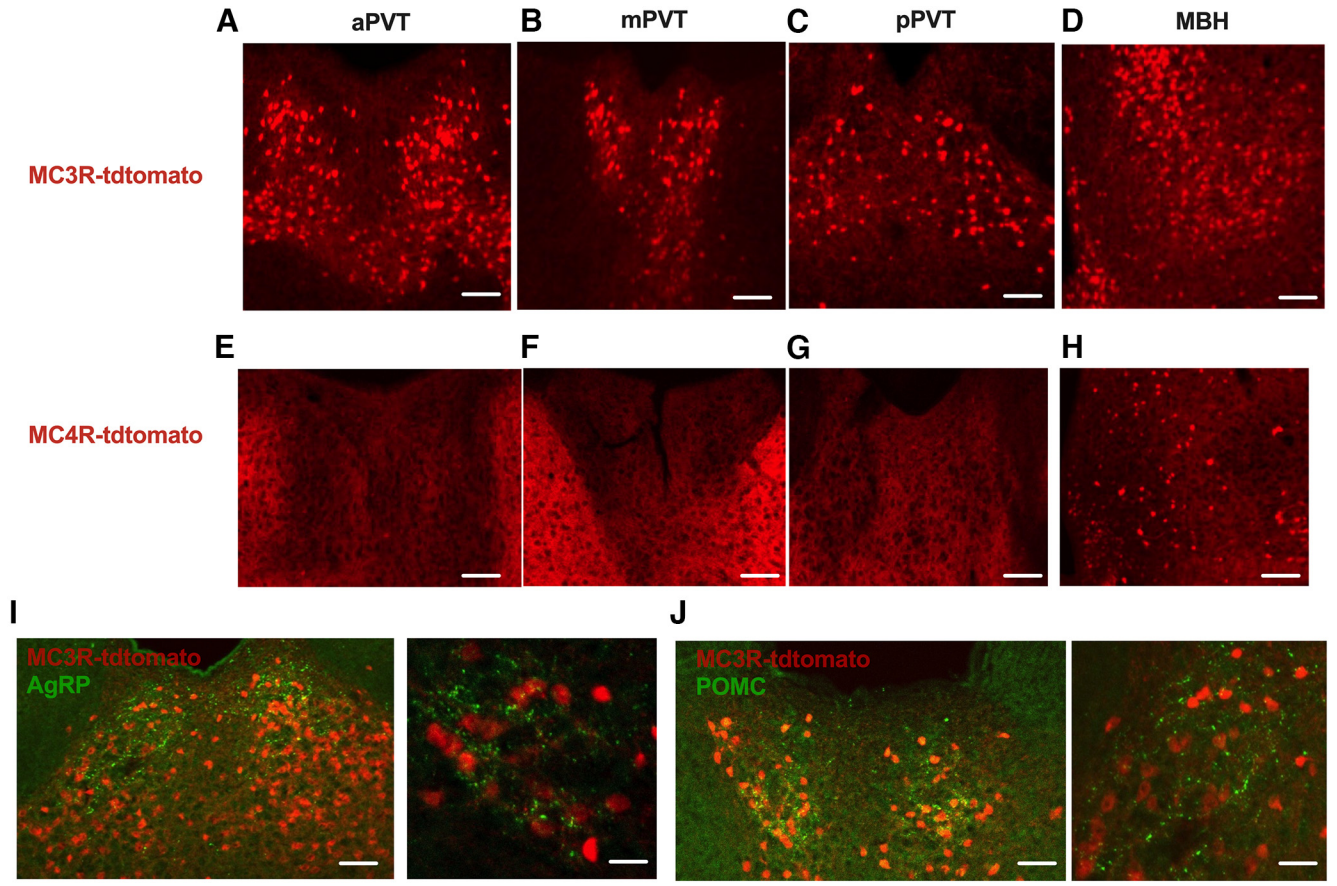

Figure 1. PVT *MC3R* neurons are functionally downstream of arcuate AgRP and POMC neurons. ***A–C***, Representative images from transgenic *MC3R*-cre x tdtomato mouse displaying *MC3R* distribution along the anterior to posterior axis of the PVT. ***D***, Image of the medial basal hypothalamus (MBH) from the same *MC3R*-tdotmato mouse. ***E–G***, Representative images from *MC4R*-cre x tdtomato mice showing lack of *MC4R*-expressing cells along the anterior to posterior axis of PVT. ***H***, Image of the MBH from the same *MC4R*-tdtomato mouse verifying the validity of this mouse line for labeling *MC4R*-containing cells. ***I***, Immunohistochemistry for AgRP in *MC3R*-Cre x tdtomato transgenic mice. ***J***, Immunohistochemistry for POMC in *MC3R*-Cre x tdtomato mice. Immunopositive fibers for AgRP and POMC overlap extensively with *MC3R* cells in PVT. Scale bars: ***A–H***, ***C*** (left), 100 um; ***I***, ***J*** (left), 100 um; ***I***, ***J*** (right), 10 um.

et al., 2013; Sternson and Atasoy, 2014; Wang et al., 2015). The paraventricular thalamus is one site that is densely innervated by AgRP and POMC neurons (Betley et al., 2013; Wang et al., 2015), although the molecular identity of the postsynaptic cells in PVT is unknown. First, to map the expression of melanocortin receptors in the PVT, we characterized the expression of *MC3R*- and *MC4R*-containing cells throughout the anterior–posterior extent of the PVT by using *MC3R-Cre* or *MC4R-Cre* mice bred with tdtomato reporter mice. Dense expression of *MC3R*-containing cells was observed throughout the PVT (Fig. 1*A–C*) and the medial-basal hypothalamus (Fig. 1*D*). However, we did not detect *MC4R*-containing cells in any region of the PVT (Fig. 1*E–G*) but detected sparse *MC4R*-containing cells localized in the medial-basal hypothalamus (Fig. 1*H*). Thus, although both *MC3R* and *MC4R* are expressed in the hypothalamus, the paraventricular thalamus exclusively contains *MC3R*-expressing cells. Next, to determine whether AgRP and POMC neurons innervate *MC3R*-containing cells in the PVT we performed immunofluorescence for both AgRP and POMC in *MC3R-Cre*; *tdtomato* reporter mice (Fig. 1*I*, *J*) (Ghamari-Langroudi et al., 2018; Sweeney et al., 2021b). PVT *MC3R* neurons were densely innervated by both AgRP and POMC immunoreactive fibers (Fig. 1*I*,*J*) throughout the extent of PVT. These results suggest a pathway connecting hypothalamic melanocortin neurons to *MC3R* cells in PVT, although further functional studies are required to establish the functional connectivity between hypothalamic melanocortin neurons and *MC3R*-containing cells in PVT.

PVT *MC3R* neurons are glutamatergic and innervate subcortical anxiety circuits

To confirm that *MC3R* mRNA is expressed within the PVT, and to identify the neurochemical identity of PVT *MC3R* neurons, we next performed dual color RNAscope fluorescent *in situ* hybridization to localize *MC3R* expression in PVT. Consistent with immunofluorescent experiments (Fig. 1), *MC3R* mRNA was observed throughout the anterior–posterior axis of PVT (Fig. 2*A*,*B*). Previous work indicates that most PVT cells are glutamatergic (Curtis et al., 2021), although this has not been confirmed for the *MC3R*-containing cells in PVT. Confirming the presumed glutamatergic nature of PVT *MC3R* neurons, we detected a high degree of colocalization of *MC3R* expression with the glutamatergic marker vGLUT2 (Fig. 2*A*) and did not colocalize *MC3R* with the GABAergic marker vGAT (Fig. 2*B*).

We next used neuroanatomical tracing approaches to map the projections of PVT *MC3R* cells. Viral vectors expressing a Cre-recombinase-dependent virus containing the mCherry fluorescent protein were targeted to the PVT in *MC3R*-Cre mice (Fig. 2*C*). Projections of PVT *MC3R* neurons were subsequently identified by immunofluorescence. Consistent with prior studies (Li et al., 2021), we identified *MC3R* PVT projections in the

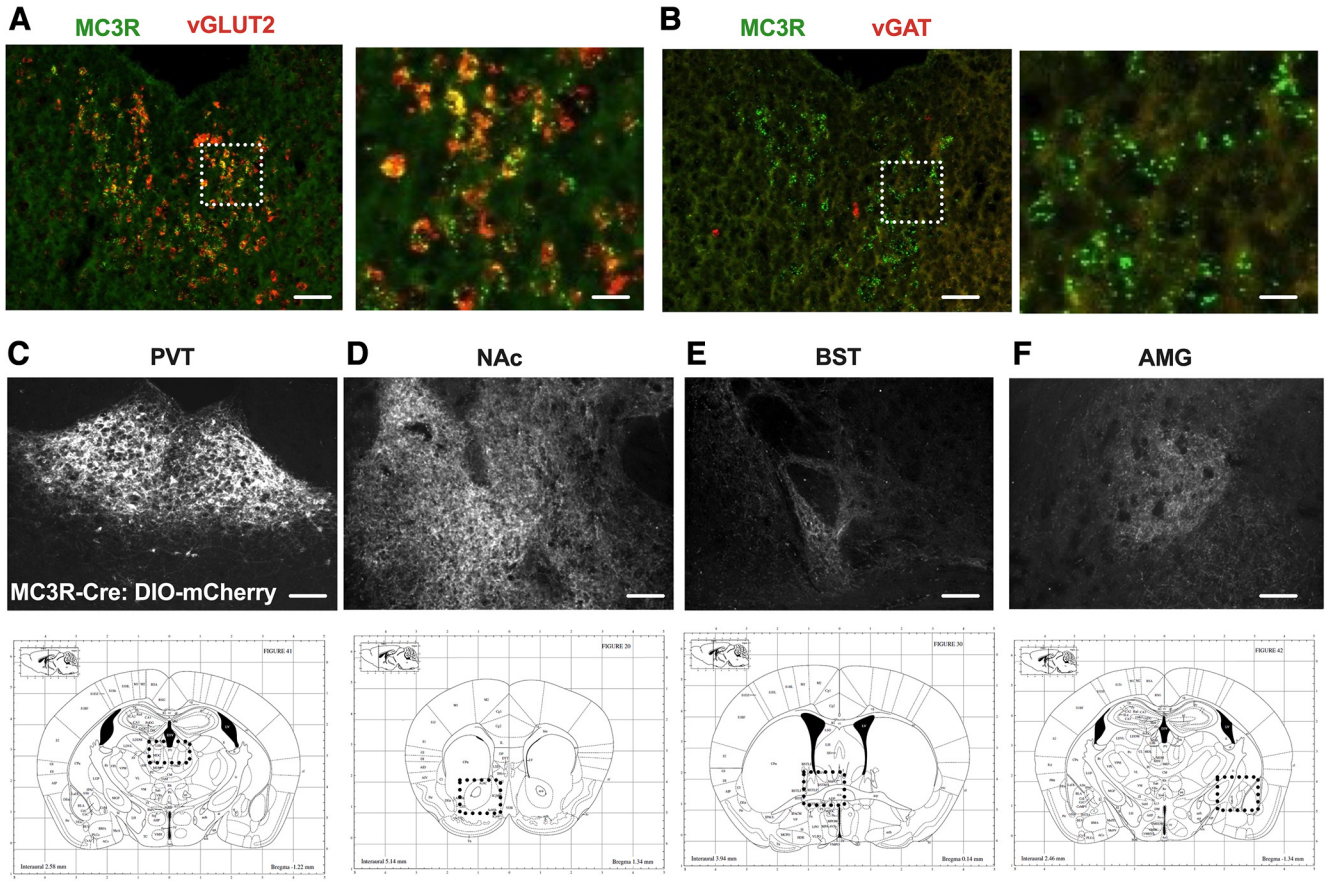

Figure 2. PVT *MC3R* neurons are glutamatergic and project to NAc, BST, and AMG. ***A***, Representative images of *MC3R* (green) and vGLUT2 (red) mRNA using RNA *in situ* hybridization in PVT. ***B***, Representative images of *MC3R* (green) and vGAT (red) mRNA using RNA *in situ* hybridization in PVT. ***C***, Viral expression of Cre-dependent virus expressing mCherry in PVT *MC3R* neurons. ***D–F***, Representative images showing projections from PVT *MC3R* neurons to downstream regions including NAc (***D***), BST (***E***), and AMG (***F***). Scale bars: ***A***, ***B*** (left), 100 um, (right) 10 um; ***C–F***, 100 um. PVT images in ***A*** and ***B*** taken from mid-/posterior PVT (bregma, −1.2). Bottom row indicates a schematic of the neuroanatomical location shown in ***C–F***. NAc (nucleus accumbens), BST (bed nucleus of the stria terminalis), AMG (amygdala).

nucleus accumbens, bed nucleus of the stria terminalis, and amygdala (Fig. 2*D–F*). Therefore, PVT *MC3R* neurons are anatomically positioned to regulate motivation and anxiety-related behavior via projections to subcortical regions critically involved in motivation, anxiety-related behavior, and reward (Fig. 2*C–F*).

PVT *MC3R* neurons are activated by satiating stimuli

Prior neuroanatomical data (Fig. 1*I,J*) suggest that PVT *MC3R* neurons may be sensitive to energy-state-related information, downstream of hypothalamic AgRP and POMC neurons. Therefore, to determine whether PVT *MC3R* neurons are sensitive to the energy state of the animal we next performed immunohistochemical analysis for c-*fos* protein in *MC3R*-Cre x tdtomato transgenic mice. Importantly, prior studies used dual RNA *in situ* hybridization for *MC3R* and mCherry to establish that this genetic targeting strategy labels bona fide *MC3R*-containing cells (Bedenbaugh et al., 2022). Thus, this approach allows for a simple (albeit indirect) strategy to map neuronal activation of *MC3R*-containing cells *in vivo*. Consistent with a role in sensing energy state, we observed increased c-*fos* protein colocalization in PVT *MC3R* neurons following refeeding after a fast (Fig. 3*A–C*). This increased colocalization was more prominent in the posterior portions of the PVT than anterior PVT, although a trend toward increased c-*fos* colocalization was also observed in the anterior PVT (Fig. 3*D,E*). In contrast, no significant difference in total c-*fos* protein expression was observed between fed *ad libitum* and refed mice in both the anterior and posterior PVT (Fig. 3*F,G*), although higher baseline c-*fos* protein levels were observed in more anterior portions of PVT.

As more PVT *MC3R* neurons coexpressed c-*fos* protein following refeeding (relative to fed *ad libitum* conditions, Fig. 3*A–C*), we next tested whether PVT *MC3R* neurons are responsive to pharmacologically induced satiety by injecting the melanocortin receptor agonist setmelanotide (1 mg/kg, i.p.) or saline in *MC3R*-Cre x tdtomato mice (Fig. 3*H–J*). Administration of setmelanotide increased the percentage of PVT *MC3R* cells coexpressing c-*fos* protein, suggesting that PVT *MC3R* neurons are more active following both physiological and pharmacological-induced satiety (Fig. 3*H–J*). However, future work is required to more fully map how changes in energy state affect the electrophysiological properties of PVT *MC3R* neurons.

PVT *MC3R* neurons are activated by aversive and anxiogenic stimuli

As PVT *MC3R* neurons project to critical neural circuitry controlling aversion and anxiety-related behavior (Fig. 2*C–F*), we hypothesized that PVT *MC3R* neurons may encode aversive and anxiogenic related information. To determine how PVT *MC3R* neuronal activity changes in awake-behaving mice during stressful stimuli, we used *in vivo* fiber photometry to record changes in calcium in PVT *MC3R* neurons (Fig. 4*A–C*). AAV viral injections of the Cre-recombinase-dependent genetically encoded calcium indicator GCAMP8m were targeted to the

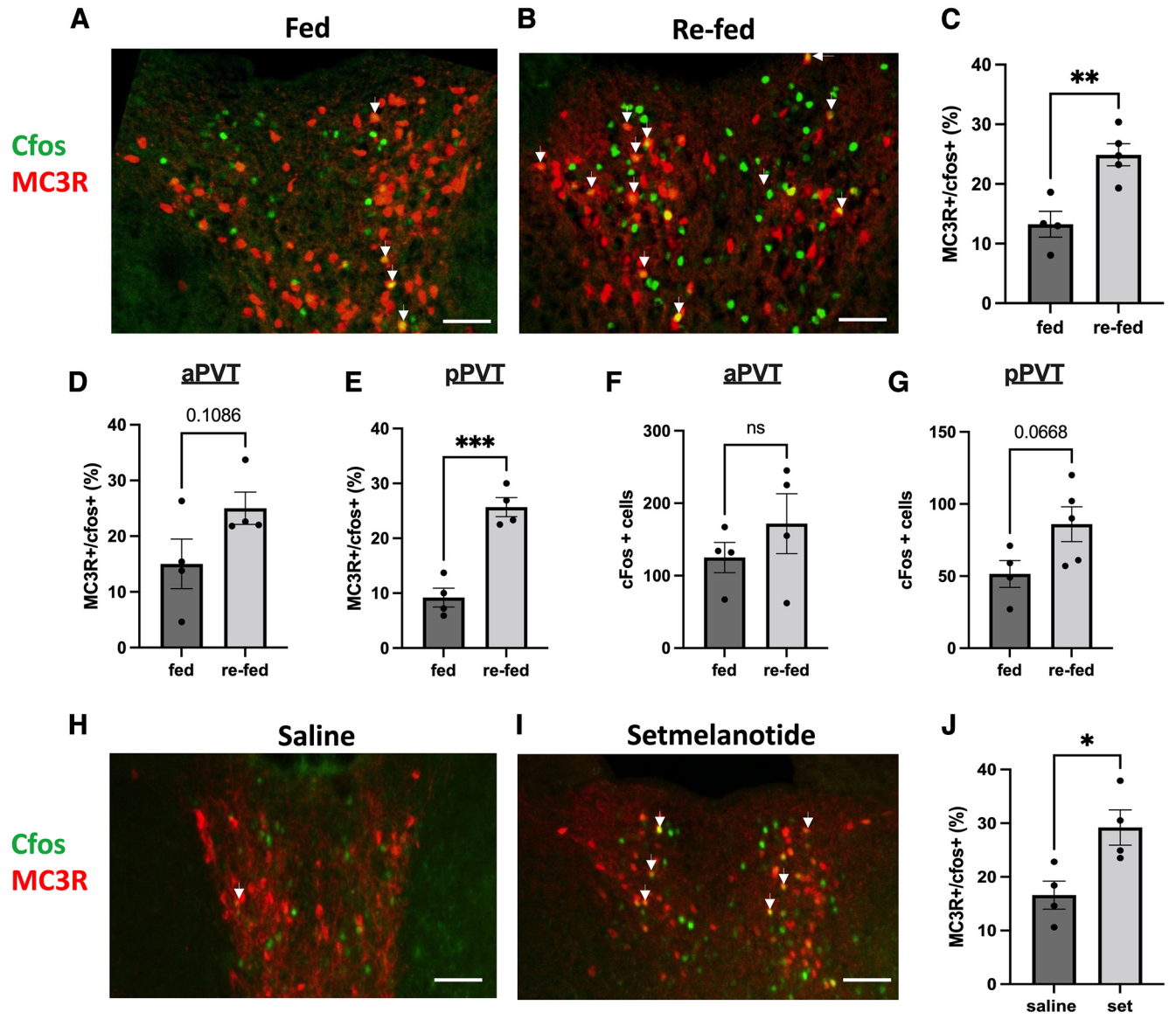

Figure 3. PVT *MC3R* neurons are activated by refeeding and melanocortin agonist treatment. ***A***, ***B***, Colocalization of c-*fos* protein in PVT *MC3R* neurons (*MC3R*-Cre x tdtomato transgenic mice) in the fed *ad libitum* state (***A***) or following 1 h of refeeding after an 18 h fast (***B***). ***C***, Quantification of the percentage of total PVT *MC3R* cells colabeled with the c-*fos* protein in the fed ($n = 4$ mice) and refed ($n = 5$ mice) state. Significantly more PVT *MC3R* cells colocalized for c-*fos* in the refed versus the fed state (Student's unpaired *t* test, $t_{(7)} = 4.12$, $p = 0.004$). ***D***, ***E***, Percentage of PVT *MC3R* cells containing c-*fos* in the anterior PVT (***D***; $t_{(6)} = 1.884$, $p = 0.108$) and posterior PVT (***E***; $t_{(6)} = 6.740$, $p = 0.0005$) in *ad libitum* fed mice and mice refed for 1 h following fasting. ***F***, Total number of c-*fos*-positive cells in the anterior portions of PVT (bregma −0.3 to −1.0) in mice fed *ad libitum* and mice refed for 1 h following fasting ($t_{(6)} = 1.009$, $p = 0.35$). ***G***, Total number of c-*fos*-positive cells in the posterior portions of PVT (bregma −1.1 to −2.0) in mice fed *ad libitum* and mice refed for 1 h following fasting ($t_{(7)} = 2.17$, $p = 0.067$). ***H***, ***I***, Representative images showing the colocalization of c-*fos* in PVT *MC3R* neurons following intraperitoneal injections of saline or setmelanotide. ***J***, Quantification of the number of *MC3R* cells colabeled with c-*fos* protein in PVT following injections of saline ($n = 4$) or the melanocortin agonist setmelantoide ($n = 4$ mice, 5 mg/kg, i.p.). Significantly more *MC3R* cells were colabeled with c-*fos* protein following setmleanotide injections relative to control saline injections (Student's unpaired *t* test, $t_{(6)} = 3.01$, $p = 0.02$). Arrows in ***A***, ***B***, ***H***, and ***I*** indicate colabeled cells. All data analyzed with unpaired Student's *t* test). ns, Not significant; $^*p < 0.05$, $^{**}p < 0.01$, $^{***}p < 0.001$. Individual data points in ***C–G*** and ***J*** indicate individual mice. Scale bars: 100 um.

PVT in *MC3R*-Cre mice (Fig. 4*A*,*B*). In the same surgical procedure, a fiber optic cannula was inserted directly into PVT to detect changes in fluorescence, which provides a readout of calcium levels in the cell, and an indirect readout of neuronal activity (Fig. 4*B*,*C*; Gunaydin et al., 2014). *MC3R* neurons were robustly activated following restraint stress, suggesting that these cells are recruited during aversive stimuli (Fig. 4*D–F*). This activation was time locked to physical restraint, increasing during physical restraint, and decreasing to baseline levels following the cessation of restraint. We next tested whether PVT *MC3R* neurons are also sensitive to other forms of stress/aversion, such as the aversive predator odor TMT (Fig. 4*G*). PVT *MC3R* neurons were robustly activated following exposure to TMT (Fig. 4*H*,*I*). In contrast to physical restraint (Fig. 4*D–F*), this neuronal activation persisted for the entire period of TMT exposure, likely reflecting the irreversibility of aversive olfactory exposure (Fig. 4*G*). Importantly, no change in neuronal activity was observed when a Kimwipe containing water was presented in the home cage of the mouse in the same manner as TMT (Fig. 4*J–M*).

Because AgRP and POMC neurons also regulate anxiety-related behavior (Dietrich et al., 2015; Li et al., 2019; Qu et al., 2020; Fang et al., 2021), and PVT circuitry has been previously

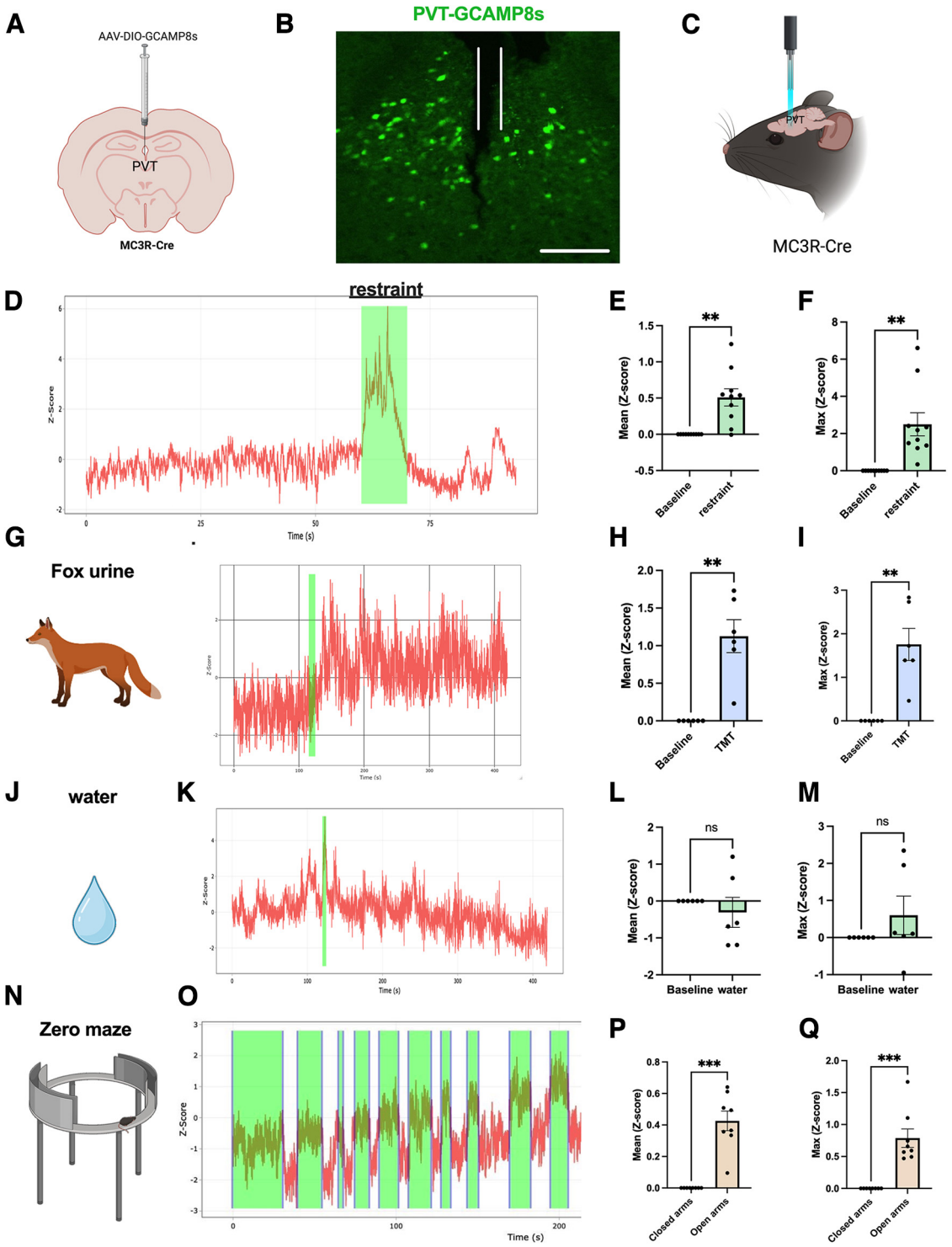

Figure 4. PVT *MC3R* neurons are activated by anxiogenic and aversive stimuli. ***A***, Viral injection strategy for expressing the genetically encoded calcium indicator GCAMP8 in PVT *MC3R* neurons. ***B***, Representative image of GCAMP8s expression in PVT *MC3R* neurons with a fiber optic cannula inserted into the PVT. Cannula trace marked in white. ***C***, Schematic depicting *in vivo* fiber photometry calcium imaging of PVT *MC3R* neuronal activity in awake, behaving mice. ***D***, Schematic of approach used for restraint stress experiments and representative trace of calcium activity (*Z*-scored) during restraint stress. Restraint period highlighted in green. ***E***, ***F***, Mean change in calcium activity during restraint versus before restraint (***E***; $t_{(9)} = 4.3$, $p = 0.002$, $n = 10$ mice), and maximum calcium activity (***F***; $t_{(9)} = 4.03$, $p = 0.003$, $n = 10$ mice) during restraint versus before restraint. ***G***, Schematic of approach used for TMT imaging experiments and representative trace of calcium activity in PVT *MC3R* neurons on introduction of the predator odor TMT. ***H***, ***I***, Mean change in calcium activity (***H***; $t_{(5)} = 5.13$, $p = 0.004$, $n = 6$ mice) and maximum calcium activity (***I***; $t_{(5)} = 4.77$, $p = 0.005$, $n = 6$ mice) before and after TMT exposure. ***J***, ***K***, Representative trace of calcium activity following the presentation of water, presented in an identical manner as TMT exposure experiments. ***L***, ***M***, Mean change in calcium activity (***L***; $t_{(5)} = 0.76$, $p = 0.48$, $n = 6$ mice) and maximum calcium activity (***M***; $t_{(5)} = 1.16$, $p = 0.30$, $n = 6$ mice) after water exposure (relative to before water exposure). ***N***, ***O***, Representative trace of calcium activity during elevated zero maze test. Time in the open arms is highlighted in green. ***P***, ***Q***, Mean change in calcium activity in the open arms versus closed arms (***P***; $t_{(7)} = 6.82$, $p = 0.0002$, $n = 8$ mice) and maximum calcium activity in the open arms versus the closed arms (***Q***; $t_{(7)} = 5.46$, $p = 0.0009$, $n = 8$ mice). Data analyzed by paired Student's *t* test; $^{**}p < 0.01$, $^{***}p < 0.001$). ns, Not significant). Data points represent individual mice. Introduction of the stimulus is highlighted in green for ***G*** and ***J***. Scale bar, ***B***, 200 um.

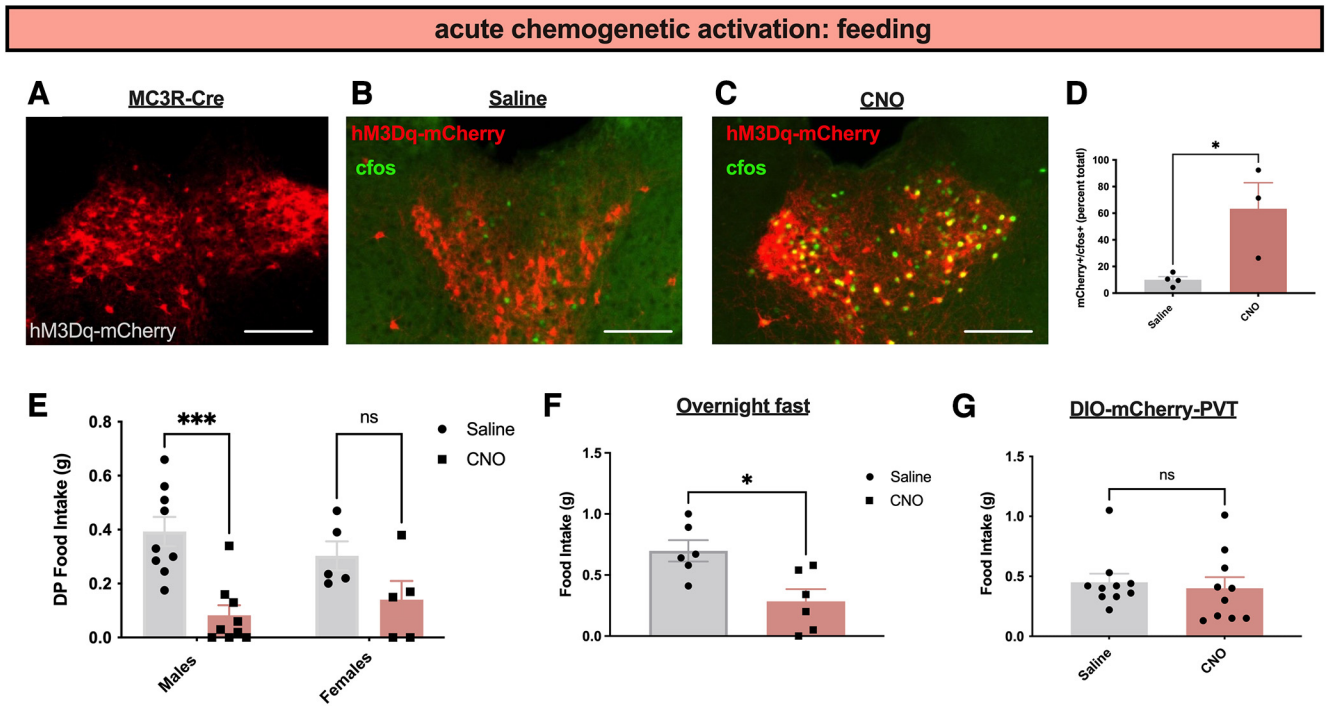

Figure 5. Activation of PVT *MC3R* neurons reduces feeding. ***A***, Representative image showing the DREADD activator hM3Dq-mCherry expression in PVT *MC3R* neurons. ***B***, ***C***, Images showing colabeling of c-*fos* immunohistochemistry with hM3Dq-mCherry virus in saline-injected mice (***B***) or mice injected with CNO (***C***). ***D***, Quantification of the percentage of *MC3R*-mCherry cells expressing c-*fos* in PVT following intraperitoneal injections of saline or CNO ($n = 4$ mice for saline group and $n = 3$ mice for CNO group; unpaired Student's t test, $t_{(4)} = 2.95$, $p = 0.04$). ***E***, Dark period food intake (2 h food intake) of male ($n = 9$) and female ($n = 5$) hM3Dq mice that were injected with saline or CNO (0.3 mg/kg, i.p.). There was no interaction between sex and food intake (2-way ANOVA, $F_{(1,24)} = 1.787$, p value $= 0.1939$) but a significant main effect of chemogenetic activation (2-way ANOVA, $F_{(1,24)} = 18.40$, p value $= 0.0003$) on food intake. ***F***, Two-hour food intake following intraperitoneal injection of CNO (0.3 mg/kg; $n = 6$ mice) or saline ($n = 6$ mice) in mice targeted with the DREADD activator hM3Dq in PVT *MC3R* neurons (Student's unpaired t test, $t_{(10)} = 3.12$, $p = 0.01$) following an overnight fast. ***G***, Two-hour food intake in *MC3R*-cre mice containing DIO-mCherry in PVT that were injected with saline or CNO ($n = 10$ male mice). No difference was detected between saline- and CNO-injected mice ($t_{(9)} = 0.38$, $p = 0.72$); $^{*}p < 0.05$, $^{***}p < 0.001$. Individual data points indicate individual mice. Scale bars: 200 um.

linked to anxiety-related behaviors (Choi and McNally, 2017; Choi et al., 2019; Kirouac, 2021; McNally, 2021; Penzo and Gao, 2021), we next tested whether PVT *MC3R* neurons are sensitive to anxiogenic environments. PVT *MC3R* neurons were robustly activated when animals entered the anxiogenic open arms of the EZM (Fig. 4*N–Q*). Neuronal activity was time locked to exposure to the anxiogenic open arms, rising as mice entered the open arms and falling as they re-entered the closed arms (Fig. 4*O*). This neuronal response repeated during each open arm entry/exit (Fig. 4*O*), suggesting an important role for these neurons in signaling anxiety-provoking stimuli.

Activation of PVT *MC3R* neurons reduces feeding and increases anxiety-related behavior

As *in vivo* imaging data demonstrate that PVT *MC3R* neurons are more active during anxiety-provoking and aversive stimuli (Fig. 4), we next used chemogenetic approaches to test the causal contribution of PVT *MC3R* neurons to feeding and anxiety-related behavior. To selectively activate PVT *MC3R* neurons, we targeted the PVT with viral injections of an AAV viral construct expressing a Cre-recombinase-dependent version of the activating DREADD hM3Dq-mCherry in *MC3R*-Cre mice (Fig. 5*A*). Immunohistochemistry analysis confirmed expression of hM3Dq-mCherry specifically in the PVT *MC3R* cells (Fig. 5*A*) and increased neuronal activity of these cells following administration of the DREADD agonist CNO (0.3 mg/kg, i.p.; Fig. 5*B–D*). To test the functional effects of activating PVT *MC3R* neurons we performed a series of feeding and anxiety-related behavioral assays in these mice. Previously, we demonstrated that chemogenetic activation of PVT *MC3R* neurons reduces feeding in mice fed *ad libitum* (Ghamari-Langroudi et al., 2018). Here, we confirmed that activation of PVT *MC3R* neurons reduces feeding in both male and female mice (Fig. 5*E*) and reduces feeding following an overnight fast (Fig. 5*F*). No difference in food intake was detected in control mCherry-expressing mice following intraperitoneal CNO injections (fed *ad libitum* dark period food intake; Fig. 5*G*).

Next, we tested whether PVT *MC3R* neurons regulate anxiety-related behavior by performing NSF and EZM tests of anxiety-related behavior in new cohorts of mice (Fig. 6). Activation of PVT *MC3R* neurons increased the latency to feed in the NSF test (Fig. 6*A*). Consistently, stimulation of PVT *MC3R* neurons decreased both time in the open arms and distance traveled in the open arms in the elevated zero maze (Fig. 6*B*,*C*), without affecting the total distance traveled (Fig. 6*D*). This effect was more significant in male mice than female animals (Fig. 6*E*,*F*). Together, these findings indicate that activation of PVT *MC3R* neurons is sufficient to reduce feeding and increase anxiety-related behavior in mice.

Inhibition of PVT *MC3R* neurons reduces anxiety-related behavior

To test whether PVT *MC3R* neurons are required for normal feeding and anxiety-related behaviors, we expressed the chemogenetic inhibitor DREADD hM4Di in PVT *MC3R* neurons (Fig. 7*A*). To validate that hM4Di inhibited the activity of PVT *MC3R*

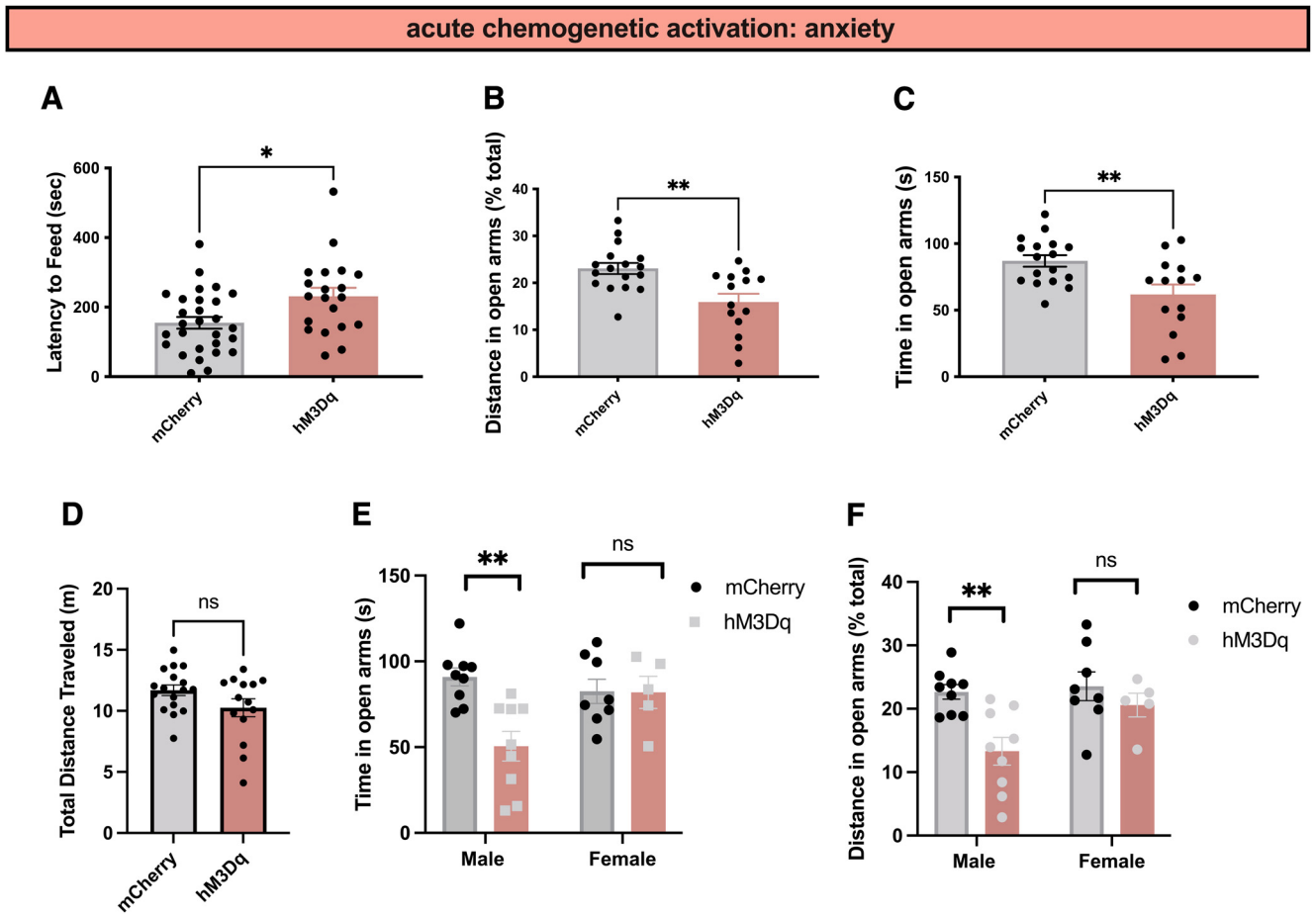

Figure 6. Activation of PVT *MC3R* neurons increases anxiety-related behavior. ***A***, Latency to feed during novelty-suppressed feeding tests in control mCherry ($n = 28$ mice) and hM3D mice ($n = 20$ mice) injected with CNO (0.3 mg/kg; Mann–Whitney test, two-tailed p value, 0.0115, Mann–Whitney $U = 160$); this figure includes mCherry and hM3D mice from cohorts 1 and 2 combined. ***B***, ***C***, Distance traveled in the open arms (***B***; Mann–Whitney test, two-tailed p value $= 0.0040$, Mann–Whitney $U = 48$) and time in the open arms (***C***; Student's unpaired t test, $t_{(29)} = 3.03$, $p = 0.005$) during the elevated zero maze test. Activation of PVT *MC3R* neurons decreased both distance traveled in the open arms (***B***) and time in the open arms (***C***) relative to control mCherry-injected mice ($n = 17$ mice in mCherry group and $n = 14$ mice in hM3Dq group). ***D***, Total distance traveled (in meters) for mCherry ($n = 17$ mice) and hM3Dq ($n = 14$ mice) mice. No statistically significant difference was observed in the total distance traveled between mCherry and hM3Dq mice following CNO administration (unpaired Students t test, $t_{(29)} = 1.75$, $p = 0.09$). ***E***, Time spent in the open arms during the elevated zero maze in mCherry male ($n = 9$ mice), mCherry female ($n = 8$), hM3Dq male ($n = 9$), and hM3Dq female ($n = 5$) mice. There is an interaction between sex and time in the open arms, with male mice, and not females, exhibiting a significant reduction in time in the open arms following activation of PVT *MC3R* neurons (2-way ANOVA, $F_{(1,27)} = 6.566$, p value $= 0.0163$). ***F***, Percentage of distance traveled in the open arms in mCherry male ($n = 9$ mice), mCherry female ($n = 8$), hM3Dq male ($n = 9$), and hM3Dq female ($n = 5$) mice (no significant interaction between sex and distance in open arms, 2-way ANOVA, $F_{(1,27)} = 2.537$, p value $= 0.1228$; main effect of hM3Dq activation, $F_{(1,27)} = 9.4$, p value $= 0.0049$). Activation of PVT *MC3R* neurons reduced distance traveled in the open arms in male, but not female, mice; $^*p < 0.05$, $^{**}p < 0.01$. Individual data points indicate individual mice.

neurons, we performed immunohistochemistry for the immediate early gene c-*fos* following administration of control saline or CNO (0.3 mg/kg, i.p.) to mice expressing hM4Di in PVT *MC3R* neurons (Fig. 7*B–D*). Administration of CNO reduced the expression of c-*fos* specifically in PVT *MC3R* neurons (Fig. 7*B–D*), confirming effective DREADD-mediated inhibition of these neurons.

Following validation of DREADD-mediated inhibition, we performed feeding and anxiety-related behavioral assays to characterize the effects of inhibiting PVT *MC3R* neurons. Acute chemogenetic inhibition of PVT *MC3R* neurons did not change feeding behavior on a regular chow diet in *ad libitum* fed conditions (Fig. 7*E*). Further, CNO injections did not alter food intake in control mCherry-injected mice (fed *ad libitum*; Fig. 7*F*). Thus, acute inhibition of PVT *MC3R* neurons does not regulate feeding behavior on a regular chow diet. To determine whether PVT *MC3R* neurons are required for regulating anxiety-related behavior we performed elevated zero maze tests following chemogenetic inhibition of PVT *MC3R* neurons (Fig. 7*G*,*H*). Inhibition of PVT *MC3R* neurons increased entries to the open arms and trended toward increasing time spent in the open arms (Fig. 7*G*,*H*). In a second cohort of mice, to confirm the effects on anxiety-related behavior, we performed open field tests of anxiety-related behavior (Fig. 7*I*). Consistent with prior elevated zero maze results, inhibition of PVT *MC3R* neurons increased the distance traveled in the center of the open field (Fig. 7*I*), with similar results obtained in both male and female mice (Fig. 7).

Given these findings, we next tested the effects of chronic PVT *MC3R* neuronal inhibition on feeding and anxiety-related behavior by targeting AAV viral vectors expressing the ion channel Kir2.1 specifically to PVT *MC3R* neurons (Fig. 8*A*; Zhu et al., 2020). To validate the effectiveness of Kir2.1 in inhibiting PVT *MC3R* neurons, we measured c-*fos* protein levels in mice expressing either control mCherry-expressing virus or Kir2.1 in PVT *MC3R* neurons (Fig. 8*B–D*). We observed several *MC3R*-mCherry; c-*fos* colocalized cells in the control group but observed few PVT *MC3R* neurons colocalized with c-*fos* in the

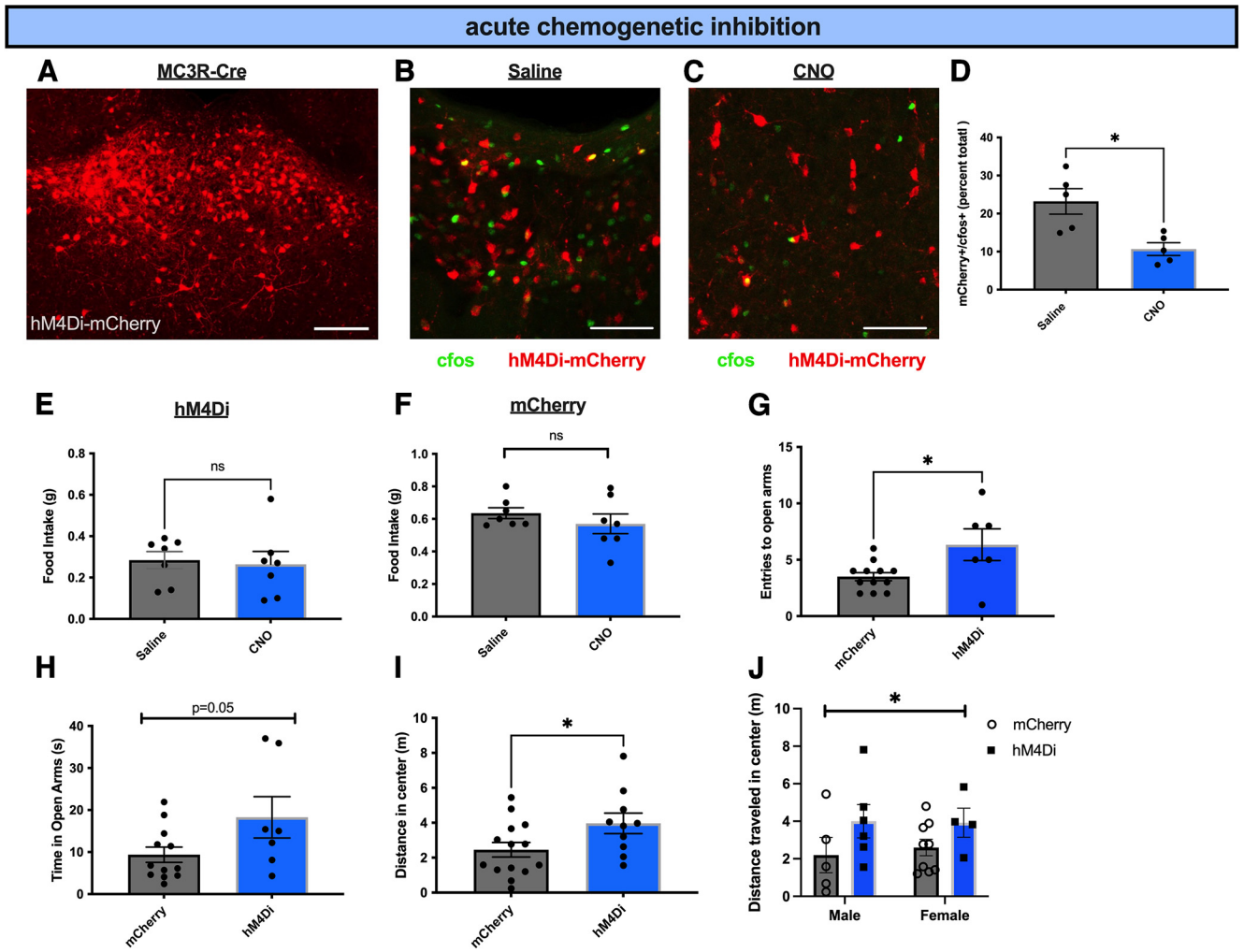

Figure 7. Inhibition of PVT *MC3R* neurons decreases anxiety-related behavior. ***A***, Representative image showing the DREADD inhibitor hM4Di-mCherry expression in PVT *MC3R* neurons. ***B***, ***C***, Representative image showing colabeling of c-*fos* immunohistochemistry with hm4di-mCherry viral expression in saline-injected mice (***B***) or CNO-injected mice (***C***). ***D***, Quantification of the percentage of PVT *MC3R* neurons activated by c-*fos* in hM4Di-mCherry-expressing mice following injections of saline or CNO ($n = 5$ mice for both saline- and CNO-injected groups, Student's unpaired *t* test, $t_{(8)} = 3.34$, $p = 0.01$). ***E***, Two-hour food intake following intraperitoneal injection of CNO (0.3 mg/kg) or saline in mice targeted with the DREADD inhibitor hM4Di in PVT *MC3R* neurons ($n = 7$ mice; Student's unpaired *t* test, $t_{(6)} = 0.02$, $p = 0.78$). ***F***, Two-hour dark period food intake in control mCherry-expressing mice following injections of saline or CNO (0.3 mg/kg, i.p.). No difference in food intake was detected between saline- and CNO-injected mice ($n = 7$ mice, Student's paired *t* test, $t_{(6)} = 1.14$, $p = 0.30$). ***G***, ***H***, Number of entries to the open arms (***G***) and time in the open arms (***H***) during the elevated zero maze. Inhibition of PVT *MC3R* neurons in hM4Di-injected mice increased the number of entries compared with mCherry mice ($n = 12$ mice in mCherry group and $n = 7$ mice in hM4Di group, Students unpaired *t* test, $t_{(16)} = 2.59$, $p = 0.019$) and trended toward increasing the time spent in the open arms ($n = 12$ mice in mCherry group and $n = 7$ mice in hM4Di group, Student's unpaired *t* test, $t_{(17)} = 2.02$, $p = 0.059$). ***I***, Distance traveled in the center of the open field arena in mCherry- or hM4Di targeted mice during open field tests. Inhibition of PVT *MC3R* neurons increased the distance traveled in the center of the open field arena compared with mCherry control injected mice ($n = 10$ mice in hM4Di group and $n = 14$ mice in mCherry group, Student's unpaired *t* test, $t_{(22)} = 2.16$, $p = 0.04$). ***J***, Total distance traveled in the center (in meters) of the OFT arena between mCherry male ($n = 5$), mCherry female ($n = 9$), hM4Di male ($n = 6$), and hM4Di female ($n = 4$) mice. There is no interaction between sex and distance traveled in the center (2-way ANOVA, $F_{(1,20)} = 6.566$, *p* value = 0.7503) but a significant main effect of hM4Di-mediated inhibition on distance traveled in the center (2-way ANOVA, $F_{(1,20)} = 4.307$, *p* value = 0.05; $^*p < 0.05$. ns, Not significant. Individual data points represent individual mice. Scale bar: ***A***, 100 um; ***B***, ***C***, 250 um.

Kir2.1 group (Fig. 8*B–D*), demonstrating successful neuronal inhibition with Kir2.1. Although acute inhibition of PVT *MC3R* neurons did not alter feeding (Fig. 7*E*), it is possible that longer-term inhibition of these neurons may produce changes in energy homeostasis. To test this hypothesis, we measured the food intake and body weight change in mice with Kir2.1 or control mCherry virus in PVT *MC3R* neurons in the weeks following viral injection. Chronic inhibition of PVT *MC3R* neurons did not alter acute or daily food intake (Fig. 8*E*,*F*). Further, control and Kir2.1-expressing mice demonstrated similar changes in body weight in the weeks following viral injection (Fig. 8*G*).

To test whether chronic inhibition of PVT *MC3R* neurons regulates anxiety-related behavior, we performed open field tests 1 month following Kir2.1 or control mCherry viral injections. Mice with Kir2.1 expression in PVT *MC3R* neurons spent more time in the center of the open field and traveled more distance in the center of the open field, without any significant change in total distance traveled (Fig. 8*H–K*). Thus, both acute and chronic inhibition of PVT *MC3R* neurons reduces anxiety-related behavior in mice without producing significant effects on feeding or body weight.

As stimulation of PVT *MC3R* neurons reduces feeding, and PVT *MC3R* neurons are activated by stressful stimuli, we tested whether these neurons are required for stress-induced anorexia. To measure the anorexigenic response to stress, we used social-isolation-induced anorexia assays, as described in our previous study (Sweeney et al., 2021b). Social isolation significantly reduced food intake in control mice and to a similar extent in

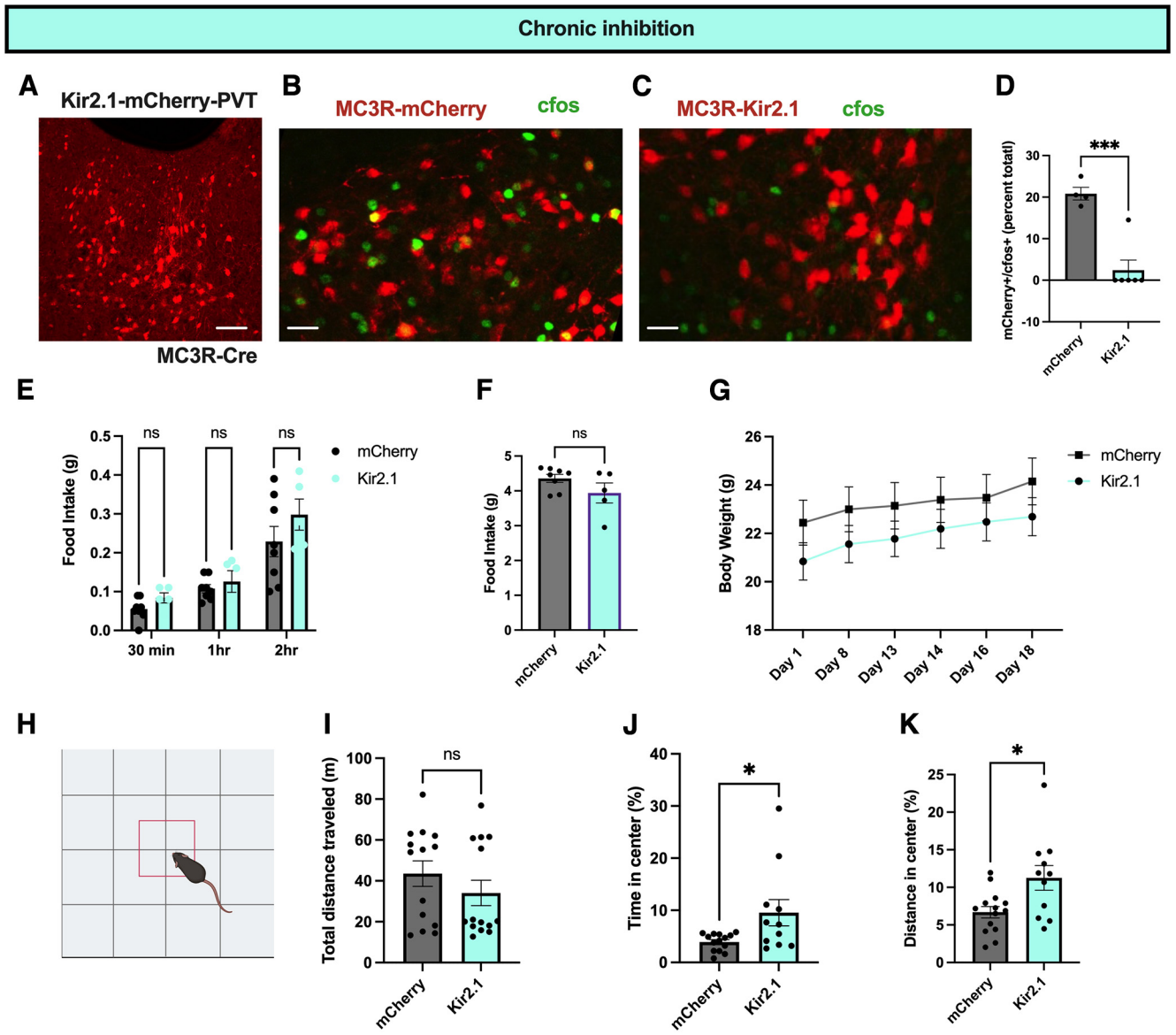

Figure 8. Chronic inhibition of PVT *MC3R* neurons reduces anxiety-related behavior. ***A***, Representative image of the viral expression of Kir2.1-mCherry in PVT *MC3R* neurons. ***B***, ***C***, Image of colabeling of *c-fos* immunohistochemistry with mCherry viral expression in control mCherry-expressing mice (***B***), or mice with Kir2.1-mCherry in PVT *MC3R* neurons. ***D***, Quantification of the percentage of PVT *MC3R* neurons containing *c-fos* in mCherry ($n = 4$) and Kir2.1-mCherry-expressing mice ($n = 4$ mice in mCherry group and $n = 6$ mice in Kir2.1 group, Student's unpaired t test, $t_{(8)} = 5.667$, p value $= 0.0005$). ***E***, Food intake of mCherry and Kir2.1 mice during the dark period in *ad libitum* fed conditions. No difference in food intake was detected between control mCherry- and Kir2.1-expressing mice ($n = 8$ mice for mCherry condition and $n = 5$ mice for Kir2.1 condition, 2-way ANOVA, main effect of viral injection condition, $F_{(1,33)} = 3.12$, $p = 0.09$). ***F***. Twenty-four-hour food intake of mCherry and Kir2.1 targeted mice during *ad libitum* access to regular chow ($n = 8$ mice in mCherry group and $n = 5$ mice in Kir 2.1 group, Student's unpaired t test, $t_{(11)} = 1.57$, $p = 0.145$). ***G***, Body weight curve of mCherry- and Kir2.1-injected mice over the course of the experiments. ***H***, Image of open field test apparatus used for open field tests. ***I***, Total distance traveled during the open field tests for both mCherry and Kir2.1 targeted mice ($n = 14$ mice in mCherry group and 11 mice in Kir2.1 groups, Mann–Whitney test, two-tailed p value $= 0.8508$, Mann–Whitney $U = 73$). ***J***, Percentage of time in the center of the open field test in mCherry-injected mice and Kir2.1-injected mice. Chronic inhibition significantly increased the percentage of time the mice spent in the center ($n = 14$ mice in mCherry group and $n = 11$ mice in Kir2.1 group; Mann–Whitney test, p value $= 0.038$, Mann–Whitney $U = 39$). ***K***, Percentage of distance traveled in the center of the open field test in mCherry-injected mice and Kir2.1-injected mice. Chronic inhibition significantly increased the percentage of distance traveled in the center of the open field test ($n = 14$ mice in mCherry group and $n = 11$ mice in Kir2.1 group; Student's unpaired t test, $t_{(23)} = 2.694$, $p = 0.01$); $^{*}p < 0.05$, $^{***}p < 0.001$. ns, Not significant. Individual data points indicate individual mice. Scale bars: ***A***, 100 um; ***B*** and ***C***, 50 um.

mice with acute or chronic inhibition of PVT *MC3R* neurons (Fig. 9). Therefore, PVT *MC3R* neurons exert a specific function in controlling anxiety-related behavior and are not required for the acute anorexigenic responses to stress.

MC3R in PVT regulates anxiety-related behavior

Chemogenetic assays demonstrate that PVT *MC3R* neurons regulate anxiety-related behavior. However, these findings do not provide information on the role of *MC3R* signaling in PVT neurons. Therefore, to specifically determine the role of *MC3R* signaling in PVT we used a novel *MC3R* floxed mouse line to specifically delete *MC3R* in the PVT in adult mice. AAV viral injections of virus expressing Cre recombinase fused to green fluorescent protein were targeted to the PVT in *MC3R* floxed mice or WT control mice (Fig. 10*A*). RNAscope *in situ* hybridization confirmed successful deletion of *MC3R* in the PVT of AAV-Cre targeted mice (Fig. 10*B*). Consistent with chemogenetic inhibition experiments, deletion of *MC3R* in PVT did not affect food

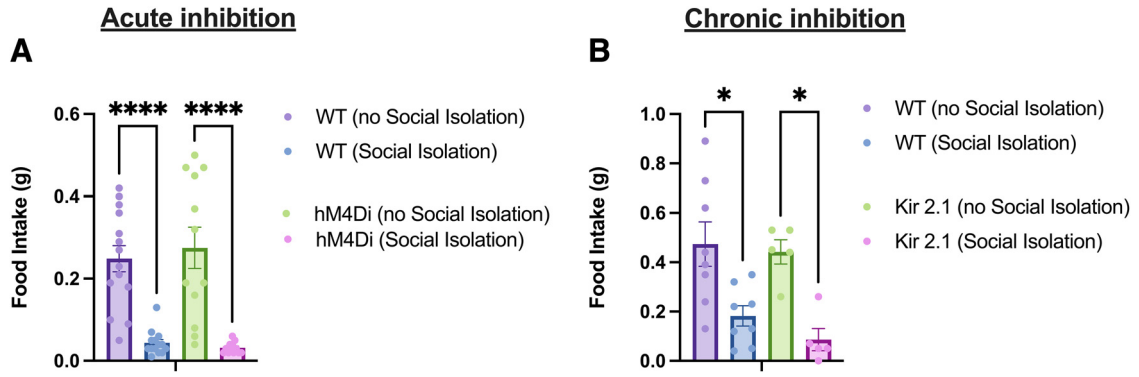

Figure 9. Inhibition of PVT *MC3R* neurons does not affect acute anorexic response to social isolation stress. ***A***, One-hour food intake in WT or hM4Di targeted mice on the day of social isolation and on the day following social isolation. Acute social isolation reduced food intake in both WT and hM4Di mice ($n = 12$ mice in hM4Di group, $n = 14$ mice in WT group; 2-way ANOVA, no significant interaction between social isolation and hM4Di-mediated inhibition, $F_{(1,48)} = 0.42$, $p = 0.52$). ***B***, One-hour food intake in WT and Kir2.1 targeted mice on the day of social isolation and the day following social isolation. Social isolation reduced food intake in both groups of mice, with no significant interaction between viral injection condition and social isolation ($n = 8$ mice in WT group and $n = 5$ mice in Kir2.1 group; 2-way ANOVA, $F_{(1,22)} = 0.22$, $p = 0.64$); $^{*}p < 0.05$, $^{****}p < 0.0001$. Data points indicate individual mice.

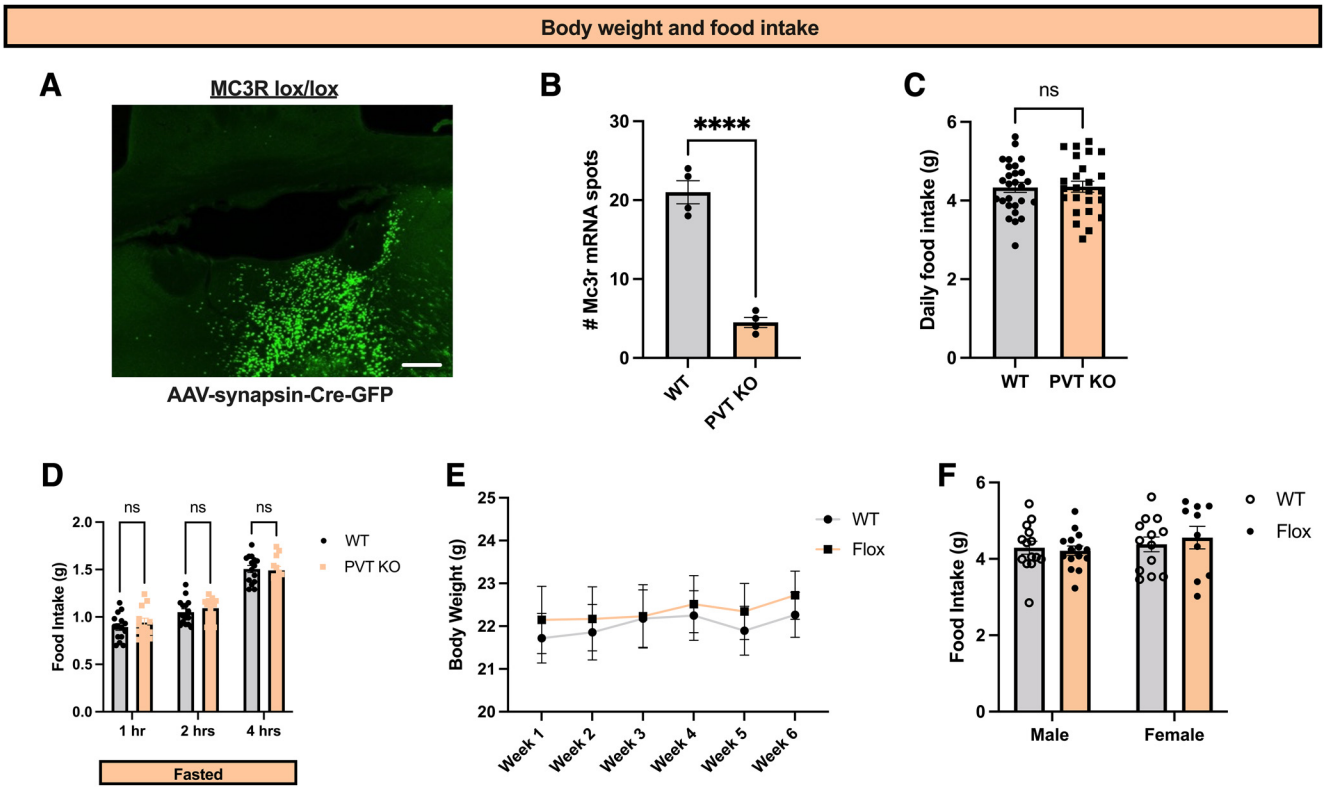

Figure 10. *MC3R* in PVT does not regulate feeding behavior on a standard chow diet. ***A***, Representative image showing viral expression of Cre-GFP in the PVT in *MC3R* lox/lox mice. ***B***, Quantification of *MC3R* mRNA levels in PVT in WT ($n = 4$ mice) and flox/flox ($n = 4$ mice) mice injected with AAV-Cre-GFP into PVT using RNA *in situ* hybridization. PVT *MC3R* KO mice showed a significant reduction in *MC3R* mRNA compared with WT mice (Student's unpaired *t* test, $t_{(6)} = 10.27$, $p < 0.0001$). ***C***, *Ad libitum* 24 h food intake for WT ($n = 27$) and flox/flox ($n = 25$) mice. No statistical difference in 24 h food intake was observed (Student's unpaired *t* test, $t_{(50)} = 0.085$, $p = 0.93$). ***D***, Acute food intake following an overnight fast in WT ($n = 15$ mice) and flox/flox mice ($n = 12$ mice). No statistical difference in food intake following an overnight fast was observed (2-way ANOVA, $F_{(2,50)} = 0.7980$, p value $= 0.4559$). ***E***, Weekly body weights of WT and flox/flox mice over the course of the experiments. ***F***, Twenty-four-hour food intake in WT male ($n = 14$), WT female ($n = 13$), flox/flox male ($n = 15$), and flox/flox female mice ($n = 10$). There is no effect of sex in this context (2-way ANOVA of interaction between sex and food intake, $F_{(1,48)} = 0.4467$, p value $= 0.5071$); $^{****}p < 0.0001$. ns, Not significant. Individual data points indicate individual mice. Scale bar, ***A***, 50 um.

intake of regular chow diet in basal conditions or following an overnight fast (Fig. 10*C*,*D*). Further, PVT *MC3R* KO and control mice demonstrated similar changes in body weight in the weeks following viral-mediated deletion (Fig. 10*E*), with similar results obtained in both male and female mice (Fig. 10*F*).

To determine the role of PVT *MC3R* signaling in anxiety-related behavior, we next performed elevated zero maze tests in mice with PVT-specific deletion of *MC3R* or control littermates (Fig. 11*A*). PVT *MC3R* KO mice entered the open arms less frequently, traveled less distance in the open arms, and trended toward spending less time in the open arms (Fig. 11*B*–*D*), with similar results obtained in both male and female mice (Fig. 11*E*). No difference in locomotor activity was observed between PVT *MC3R* KO and WT mice, indicating that these changes were not

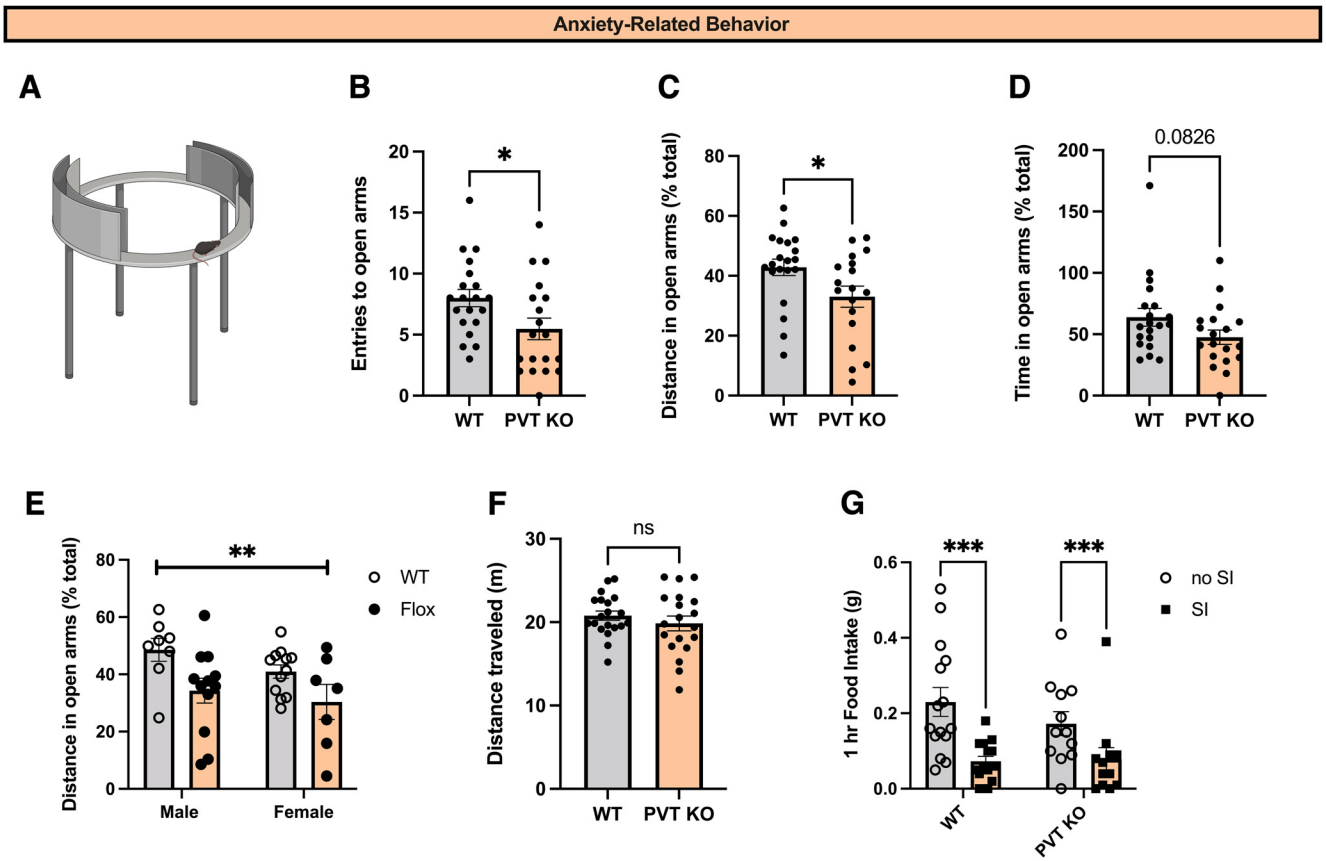

Figure 11. *MC3R* in PVT regulates anxiety-related behavior. ***A***, Image of elevated zero maze apparatus ***B***, Total number of entries to the open arms during the EZM test in WT ($n = 20$ mice) and flox/flox ($n = 19$ mice) mice. Deletion of *MC3R* from PVT significantly reduced the total number of entries to the open arms during the EZM test (Mann–Whitney test, two-tailed p value $= 0.0223$, Mann–Whitney $U = 109.5$). ***C***, Distance traveled in the open arms of the EZM in WT ($n = 20$) and flox/flox ($n = 19$) mice as a percentage of the total distance traveled. Deletion of *MC3R* from PVT significantly decreased the percentage of the distance traveled in the open arms of the EZM test (Mann–Whitney test, two-tailed p value $= 0.0208$, Mann–Whitney $U = 108$). ***D***, Time spent in the open arms of the EZM in WT ($n = 20$) and flox/flox ($n = 19$) mice. Deletion of *MC3R* from PVT did not significantly reduce the percentage of time spent in the open arms, although a trend was observed (Mann–Whitney test, two-tailed p value $= 0.0826$, Mann–Whitney $U = 128$). ***E***, Distance traveled in the open arms of the EZM as a percentage of the total distance traveled in WT male ($n = 8$), WT female ($n = 12$), flox/flox male ($n = 12$), and flox/flox female ($n = 7$) mice. There is no effect of sex in this context (2-way ANOVA of interaction between sex and percentage of distance in the open arms, $F_{(1,35)} = 0.7593$, p value $= 0.7593$) but a main overall effect of *MC3R* deletion (2-way ANOVA, main effect of genotype, $F_{(1,35)} = 8.7$, $p = 0.005$). ***F***, Distance traveled (in meters) during EZM experiment in WT ($n = 20$) and flox/flox ($n = 19$) mice. No statistical difference was observed between WT and flox/flox mice in total distance traveled (Student's unpaired t test, $t_{(37)} = 0.91$, $p = 0.37$). ***G***, One-hour food intake on the day of social isolation and the day following social isolation. Deletion of *MC3R* in PVT did not alter the acute anorexic response to social isolation (2-way ANOVA, interaction between genotype and social isolation, $F_{(1,50)} = 1.1$, $p = 0.29$); $^{*}p < 0.05$, $^{**}p < 0.01$, $^{***}p < 0.001$. ns, Not significant. Individual data points indicate individual mice.

secondary to altered locomotor activity (Fig. 11*F*). Given that PVT *MC3R* neurons are activated by stressful stimuli (Fig. 4), and activation of these neurons reduces food intake (Fig. 5), we next tested whether *MC3R* signaling in PVT regulates the acute anorexic response to stress. Consistent with acute and chronic neuronal inhibition studies (Fig. 9), the deletion of *MC3R* in PVT did not alter the acute anorexic responses to social isolation stress (Fig. 11*G*). Together, *MC3R* signaling in PVT is important for regulating anxiety-like behavior but is not required for the regulation of feeding in basal conditions or the acute anorexic response to social isolation stress.

Discussion

The paraventricular thalamus is ideally positioned to integrate exteroceptive and interoceptive information and regulate behavior in response to changing conditions (Kirouac, 2015; McGinty and Otis, 2020; Penzo and Gao, 2021). PVT is innervated by hypothalamic and hindbrain regions critical for regulation of energy homeostasis. For example, arcuate nucleus AgRP neurons (Wang et al., 2015), lateral hypothalamic orexin neurons (Meffre et al., 2019), and neurons in the ventral medial hypothalamus (Zhang et al., 2020), zona incerta (Zhang and van den Pol, 2017), and the parasubthalamic nucleus (Zhang and van den Pol, 2017) all directly regulate feeding via projections to PVT. Further, the PVT receives inputs from hindbrain neurons in the nucleus of the solitary tract (Dumont et al., 2022) and parabrachial nucleus (Zhu et al., 2022) which may communicate meal-derived satiety signals from the gut directly to PVT. Presumably, hypothalamic and hindbrain projections to PVT act to convey physiological state information to PVT neurons, which directly innervate cortical and subcortical structures controlling behavioral approach/avoidance and motivation (Kelley et al., 2005). PVT neurons are also sensitive to external stressors (Kirouac, 2015, 2021; Penzo et al., 2015; Zhu et al., 2018; Campus et al., 2019; Barson et al., 2020) and are innervated by cortical, hippocampal, and subcortical regions conveying external danger and contextual information (Li and Kirouac, 2012). This anatomic structure supports a conceptual framework for the PVT in integrating internal and external state information and communicating this information to subcortical and cortical structures to initiate an appropriate behavioral response (Kelley et al., 2005). Consistent with this

interpretation, prior studies indicate that PVT circuitry is critical for prioritizing motivated behaviors toward the underlying need state of the animals (Choi and McNally, 2017; Choi et al., 2019; Meffre et al., 2019; Otis et al., 2019; Horio and Liberles, 2021; Penzo and Gao, 2021).

We propose here that PVT cells containing the *MC3R* represent a subset of PVT neurons with a specialized role in communicating energy state information with subcortical structures controlling approach/avoidance behaviors, as has been demonstrated for other PVT cell types with dedicated roles in sensing changes in glucose homeostasis (Labouèbe et al., 2016; Sofia Beas et al., 2020; Kessler et al., 2021). Such a circuit architecture would facilitate adaptive decision-making and behavioral approaches in the face of changing internal and external conditions (McGinty and Otis, 2020; Penzo and Gao, 2021). The neuroanatomical and behavioral evidence presented here suggests that PVT *MC3R* neurons likely mediate their effects by relaying energy state information from hypothalamic melanocortin neurons (Fig. 1) to downstream cells in the nucleus accumbens, bed nucleus of the stria terminalis, and amygdala (Fig. 2). However, further work is required to map the functional connections between hypothalamic (arcuate nucleus AgRP and POMC neurons) and hindbrain (nucleus of the solitary tract POMC neurons) melanocortin neurons and *MC3R* neurons in PVT and to determine the specific function of each of the PVT *MC3R* projection pathways. Additionally, future work should establish the relationship between signals of satiety [i.e., CCK, PYY (peptide tyrosine-tyrosine), GLP1 (glucagon-like peptide-1] and hunger (i.e., ghrelin) and the activity of PVT *MC3R* neurons.

PVT *MC3R* neurons bidirectionally control anxiety-related behavior, with neuronal activation increasing anxiety-related behaviors and inhibition decreasing anxiety-related behaviors (Fig. 5–8). Importantly, these effects are physiologically relevant as PVT *MC3R* neurons are robustly activated by aversive stimuli and exposure to anxiogenic environments (Fig. 4). Further, deletion of *MC3R* in the PVT alters anxiety-related behavior (Fig. 11), indicating a functional role for *MC3R* signaling in PVT in modulating anxiety state. This finding is consistent with a prior report indicating increased anxiety-related behavior in global *MC3R* KO mice (Sweeney et al., 2021b) and suggests that PVT is one region mediating the anxiogenic effects of *MC3R* deletion. Here, it is important to note that it is impossible to infer directionality from genetic loss of function studies (i.e., global or site-specific deletion of *MC3R*) because the dynamics of melanocortin peptide release in terminal regions, including PVT, are unknown. For example, the endogenous melanocortin receptor agonist aMSH is proposed to stimulate *MC3R* activity, whereas the antagonist AgRP likely inhibits receptor function. As AgRP mRNA levels are elevated in the fasted state, and aMSH levels are elevated in the sated state, the energy state of the animal may profoundly alter the physiological state of *MC3R* activity in PVT *MC3R* neurons. Thus, *MC3R* signaling in PVT may bidirectionally control anxiety-related behavior depending on the energy state of the animal, leading to anxiolytic effects in the fasted state (via AgRP-mediated inhibition of PVT *MC3R* neurons) or anxiogenic effects in the fed state (via aMSH-mediated activation of PVT *MC3R* neurons). Further work is required to determine the dynamics of endogenous melanocortin release in postsynaptic sites, such as PVT, and to decipher the intracellular signaling pathways by which melanocortins regulate the activity of *MC3R*-containing cells in PVT.

The previous literature supports an important role for PVT circuitry in regulating anxiety-related behavior (Kirouac, 2021), and emerging evidence suggests that posterior portions of PVT are particularly important for regulating anxiety-related behavior (relative to anterior PVT; Barson and Leibowitz, 2015; Barson et al., 2020). However, the direction of the observed effects is not always consistent. For example, activation of posterior PVT projections to the amygdala increases behavioral measures of fear and/or anxiety (Do-Monte et al., 2015; Penzo et al., 2015; Pliota et al., 2020), whereas inhibitory infusions of GABA agonists into the pPVT also increase measures of anxiety in the elevated plus maze in rats (Barson and Leibowitz, 2015). Thus, distinct PVT circuitry appear to exert unique effects on anxiety-related behavior depending on the specific downstream circuitry and/or the targeted cell types.

In contrast with the pPVT, the specific role of anterior PVT (aPVT) in anxiety-related behavior is less well established, and the direction of effects on anxiety is again inconsistent across studies (Barson et al., 2020). For instance, aPVT projections to the amygdala and nucleus accumbens promoted anxiety-related and aversive behaviors in one study (Do-Monte et al., 2017), whereas others have reported reduced anxiety-related behavior following activation of aPVT projections to nucleus accumbens (Cheng et al., 2018). Further work is required to establish the importance of anterior versus posterior PVT in the *MC3R*-related effects reported here. However, we propose that cell-type-specific approaches may be critical for dissecting PVT function, as distinct cell types likely exert specific control over behavior. Advances in understanding the molecular identity of PVT neurons, such as the recently published single nuclei transcriptome of PVT (Gao et al., 2023), should aid in defining the function of distinct PVT cell types and circuits in behavioral control. In addition to the anatomic specificity of PVT circuits, it is important to note that PVT neurons may be more active during the dark period (active period in rodents; Kolaj et al., 2012), and manipulations of PVT may have different effects depending on the time of day (McDevitt and Graziane, 2019; Barson and Leibowitz, 2015; Li et al., 2010a, b). Future work is required to map the temporal kinetics of PVT *MC3R* neurons across the light/dark cycle and to establish the effect of PVT *MC3R* manipulations during the dark period.

The neural circuitry regulating energy homeostasis is bidirectionally connected with neural circuitry controlling mood and anxiety-related behavior (Sweeney and Yang, 2017). These circuit interactions are likely involved in the underlying etiology of neuropsychiatric eating disorders and the established link among obesity, anxiety, and depressive disorders (Luppino et al., 2010; Blasco et al., 2020; Fulton et al., 2022). Here, we identify PVT neurons containing the *MC3R* as a molecularly defined cell type positioned between hypothalamic neurons communicating energy status (Fig. 1) and subcortical circuitry controlling anxiety-related behavior (Fig. 2). These findings add to the literature implicating PVT circuitry in anxiety-related behavior and provide a cellular entry point for further investigation of the neural circuit mechanisms mediating communication between energy state and emotional circuitry. Ultimately, a more comprehensive understanding of the molecular nature of this circuitry may provide therapeutic strategies for treating neuropsychiatric eating disorders and/or psychiatric conditions associated with obesity.

References

Aponte Y, Atasoy D, Sternson SM (2011) AGRP neurons are sufficient to orchestrate feeding behavior rapidly and without training. Nat Neurosci 14:351–355.

Barson JR, Leibowitz SF (2015) GABA-induced inactivation of dorsal midline thalamic subregions has distinct effects on emotional behaviors. Neurosci Lett 609:92–96.

Barson JR, Mack NR, Gao WJ (2020) The paraventricular nucleus of the thalamus is an important node in the emotional processing network. Front Behav Neurosci 14:598469.

Bedenbaugh MN, Brener SC, Maldonado J, Lippert RN, Sweeney P, Cone RD, Simerly RB (2022) Organization of neural systems expressing melanocortin-3 receptors in the mouse brain: evidence for sexual dimorphism. J Comp Neurol 530:2835–2851.

Betley JN, Cao ZFH, Ritola KD, Sternson SM (2013) Parallel, redundant circuit organization for homeostatic control of feeding behavior. Cell 155:1337–1350.

Betley JN, Xu S, Cao ZFH, Gong R, Magnus CJ, Yu Y, Sternson SM (2015) Neurons for hunger and thirst transmit a negative-valence teaching signal. Nature 521:180–185.

Beutler LR, Chen Y, Ahn JS, Lin YC, Essner RA, Knight ZA (2017) Dynamics of gut-brain communication underlying hunger. Neuron 96:461–475.e5.

Blasco BV, García-Jiménez J, Bodoano I, Gutiérrez-Rojas L (2020) Obesity and depression: its prevalence and influence as a prognostic factor: a systematic review. Psychiatry Investig 17:715–724.

Burnett CJ, Li C, Webber E, Tsaousidou E, Xue SY, Brüning JC, Krashes MJ (2016) Hunger-driven motivational state competition. Neuron 92:187–201.

Burnett CJ, Funderburk SC, Navarrete J, Sabol A, Liang-Guallpa J, Desrochers TM, Krashes MJ (2019) Need-based prioritization of behavior. Elife 8:e44527.

Butler AA, Kesterson RA, Khong K, Cullen MJ, Pelleymounter MA, Dekoning J, Baetscher M, Cone RD (2000) A unique metabolic syndrome causes obesity in the melanocortin-3 receptor-deficient mouse. Endocrinology 141:3518–3521.

Campus P, Covelo IR, Kim Y, Parsegian A, Kuhn BN, Lopez SA, Neumaier JF, Ferguson SM, Solberg Woods LC, Sarter M, Flagel SB (2019) The paraventricular thalamus is a critical mediator of top down control of cuemotivated behavior in rats. Elife 8:e49041.

Chen Y, Lin YC, Kuo TW, Knight ZA (2015) Sensory detection of food rapidly modulates arcuate feeding circuits. Cell 160:829–841.

Cheng J, Wang J, Ma X, Ullah R, Shen Y, Zhou YD (2018) Anterior paraventricular thalamus to nucleus accumbens projection is involved in feeding behavior in a novel environment. Front Mol Neurosci 11:202.

Choi EA, McNally GP (2017) Paraventricular thalamus balances danger and reward. J Neurosci 37:3018–3029.

Choi EA, Jean-Richard-Dit-Bressel P, Clifford CWG, McNally GP (2019) Paraventricular thalamus controls behavior during motivational conflict. J Neurosci 39:4945–4958.

Cone RD (2005) Anatomy and regulation of the central melanocortin system. Nat Neurosci 8:571–578.

Cone RD (2006) Studies on the physiological functions of the melanocortin system. Endocr Rev 27:736–749.

Cowley MA, Smart JL, Rubinstein M, Cerdán MG, Diano S, Horvath TL, Cone RD, Low MJ (2001) Leptin activates anorexigenic POMC neurons through a neural network in the arcuate nucleus. Nature 411:480–484.

Curtis GR, Oakes K, Barson JR (2021) Expression and distribution of neuropeptide-expressing cells throughout the rodent paraventricular nucleus of the thalamus. Front Behav Neurosci 14:634163.

Dietrich MO, Zimmer MR, Bober J, Horvath TL (2015) Hypothalamic Agrp neurons drive stereotypic behaviors beyond feeding. Cell 160:1222–1232.

Do-Monte FH, Quiñones-Laracuente K, Quirk GJ (2015) A temporal shift in the circuits mediating retrieval of fear memory. Nature 519:460–463.

Do-Monte FH, Minier-Toribio A, Quiñones-Laracuente K, Medina-Colón EM, Quirk GJ (2017) Thalamic regulation of sucrose seeking during unexpected reward omission. Neuron 94:388–400.e4.

Dumont C, Li G, Castel J, Luquet S, Gangarossa G (2022) Hindbrain catecholaminergic inputs to the paraventricular thalamus scale feeding and metabolic efficiency in stress-related contexts. J Physiol 600:2877–2895.

Farooqi IS, Yeo GSH, Keogh JM, Aminian S, Jebb SA, Butler G, Cheetham T, O'Rahilly S (2000) Dominant and recessive inheritance of morbid obesity associate with melanocortin 4 receptor deficiency. J Clin Invest 106:271–279.

Farooqi IS, Keogh JM, Yeo GSH, Lank EJ, Cheetham T, O'Rahilly S (2003) Clinical spectrum of obesity and mutations in the melanocortin 4 receptor gene. N Engl J Med 348:1085–1095.

Fang X, Jiang S, Wang J, Bai Y, Kim CS, Blake D, Weintraub NL, Lei Y, Lu XY (2021) Chronic unpredictable stress induces depression-related behaviors by suppressing AgRP neuron activity. Mol Psychiatry 26:2299–2315.

Fenselau H, Campbell JN, Verstegen AMJ, Madara JC, Xu J, Shah BP, Resch JM, Yang Z, Mandelblat-Cerf Y, Livneh Y, Lowell BB (2017) A rapidly acting glutamatergic ARC→PVH satiety circuit postsynaptically regulated by α-MSH. Nat Neurosci 20:1189.

Fulton S, Décarie-Spain L, Fioramonti X, Guiard B, Nakajima S (2022) The menace of obesity to depression and anxiety prevalence. Trends Endocrinol Metab 33:18–35.

Garfield AS, Lam DD, Marston OJ, Przydzial MJ, Heisler LK (2009) Role of central melanocortin pathways in energy homeostasis. Trends Endocrinol Metab 20:203–215.

Garfield AS, Li C, Madara JC, Shah BP, Webber E, Steger JS, Campbell JN, Gavrilova O, Lee CE, Olson DP, Elmquist JK, Tannous BA, Krashes MJ, Lowell BB (2015) A neural basis for melanocortin-4 receptor-regulated appetite. Nat Neurosci 18:863–871.

Ghamari-Langroudi M, Digby GJ, Sebag JA, Millhauser GL, Palomino R, Matthews R, Gillyard T, Panaro BL, Tough IR, Cox HM, Denton JS, Cone RD (2015) G-protein-independent coupling of *MC4R* to Kir7.1 in hypothalamic neurons. Nature 520:94–98.

Ghamari-Langroudi M, Cakir I, Lippert RN, Sweeney P, Litt MJ, Ellacott KLJ, Cone RD (2018) Regulation of energy rheostasis by the melanocortin-3 receptor. Sci Adv 4:eaat0866.

Gao C, Gohel CA, Leng Y, Ma J, Goldman D, Levine AJ, Penzo MA (2023) Molecular and spatial profiling of the paraventricular nucleus of the thalamus. Elife 12:e81818.

Gunaydin LA, Grosenick L, Finkelstein JC, Kauvar IV, Fenno LE, Adhikari A, Lammel S, Mirzabekov JJ, Airan RD, Zalocusky KA, Tye KM, Anikeeva P, Malenka RC, Deisseroth K (2014) Natural neural projection dynamics underlying social behavior. Cell 157:1535–1551.

Hay PJ, Touyz S, Sud R (2012) Treatment for severe and enduring anorexia nervosa: a review. Aust N Z J Psychiatry 46:1136–1144.

Herpertz-Dahlmann B, Holtkamp K, Konrad K (2012) Eating disorders: anorexia and bulimia nervosa. Handb Clin Neurol 106:447–462.

Heydendael W, Sharma K, Iyer V, Luz S, Piel D, Beck S, Bhatnagar S (2011) Orexins/hypocretins act in the posterior paraventricular thalamic nucleus during repeated stress to regulate facilitation to novel stress. Endocrinology 152:4738–4752.

Hill-Bowen LD, Flannery JS, Poudel R (2020) Paraventricular thalamus activity during motivational conflict highlights the nucleus as a potential constituent in the neurocircuitry of addiction. J Neurosci 40:726–728.

Horio N, Liberles SD (2021) Hunger enhances food-odour attraction through a neuropeptide Y spotlight. Nature 592:262–266.

Huszar D, Lynch CA, Fairchild-Huntress V, Dunmore JH, Fang Q, Berkemeier LR, Gu W, Kesterson RA, Boston BA, Cone RD, Smith FJ, Campfield LA, Burn P, Lee F (1997) Targeted disruption of the melanocortin-4 receptor results in obesity in mice. Cell 88:131–141.

Kelley AE, Baldo BA, Pratt WE (2005) A proposed hypothalamic-thalamic-striatal axis for the integration of energy balance, arousal, and food reward. J Comp Neurol 493:72–85.

Keski-Rahkonen A, Hoek HW, Susser ES, Linna MS, Sihvola E, Raevuori A, Bulik CM, Kaprio J, Rissanen A (2007) Epidemiology and course of anorexia nervosa in the community. Am J Psychiatry 164:1259–1265.

Kessler S, Labouèbe G, Croizier S, Gaspari S, Tarussio D, Thorens B (2021) Glucokinase neurons of the paraventricular nucleus of the thalamus sense glucose and decrease food consumption. iScience 24:103122.

Kirouac GJ (2015) Placing the paraventricular nucleus of the thalamus within the brain circuits that control behavior. Neurosci Biobehav Rev 56:315–329.

Kirouac GJ (2021) The paraventricular nucleus of the thalamus as an integrating and relay node in the brain anxiety network. Front Behav Neurosci 15:627633.

Kolaj M, Zhang L, Rønnekleiv OK, Renaud LP (2012) Midline thalamic paraventricular nucleus neurons display diurnal variation in resting membrane potentials, conductances, and firing patterns *in vitro*. J Neurophysiol 107:1835–1844.

Krashes MJ, Koda S, Ye CP, Rogan SC, Adams AC, Cusher DS, Maratos-Flier E, Roth BL, Lowell BB (2011) Rapid, reversible activation of AgRP neurons drives feeding behavior in mice. J Clin Invest 121:1424–1428.

Krashes MJ, Shah BP, Koda S, Lowell BB (2013) Rapid versus delayed stimulation of feeding by the endogenously released agRP neuron mediators GABA, NPY, and AgRP. Cell Metab 18:588–595.

Krashes MJ, Lowell BB, Garfield AS (2016) Melanocortin-4 receptor-regulated energy homeostasis. Nat Neurosci 19:206–219.

Labouèbe G, Boutrel B, Tarussio D, Thorens B (2016) Glucose-responsive neurons of the paraventricular thalamus control sucrose-seeking behavior. Nat Neurosci 19:999–1002.

Lam BYH, et al. (2021) *MC3R* links nutritional state to childhood growth and the timing of puberty. Nature 599:436–441.

Lee EJ, Hanchate NK, Kondoh K, Tong APS, Kuang D, Spray A, Ye X, Buck LB (2020) A psychological stressor conveyed by appetite-linked neurons. Sci Adv 6:eaay5366.

Levine OB, Skelly MJ, Miller JD, Rivera-Irizarry JK, Rowson SA, DiBerto JF, Rinker JA, Thiele TE, Kash TL, Pleil KE (2021) The paraventricular thalamus provides a polysynaptic brake on limbic CRF neurons to sex-dependently blunt binge alcohol drinking and avoidance behavior in mice. Nat Commun 12:5080.

Li C, Hou Y, Zhang J, Sui G, Du X, Licinio J, Wong ML, Yang Y (2019) AGRP neurons modulate fasting-induced anxiolytic effects. Transl Psychiatry 9:111.

Li S, Kirouac GJ (2012) Sources of inputs to the anterior and posterior aspects of the paraventricular nucleus of the thalamus. Brain Struct Funct 217:257–273.

Li S, Dong X, Kirouac GJ (2021) Extensive divergence of projections to the forebrain from neurons in the paraventricular nucleus of the thalamus. Brain Struct Funct 226:1779–1802.

Li Y, Li S, Wei C, Wang H, Sui N, Kirouac GJ (2010a) Changes in emotional behavior produced by orexin microinjections in the paraventricular nucleus of the thalamus. Pharmacol Biochem Behav 95:121–128.

Li Y, Li S, Wei C, Wang H, Sui N, Kirouac GJ (2010b) Orexins in the paraventricular nucleus of the thalamus mediate anxiety-like responses in rats. Psychopharmacology (Berl) 212:251–265.

Liu J, Garza JC, Truong HV, Henschel J, Zhang W, Lu XY (2007) The melanocortinergic pathway is rapidly recruited by emotional stress and contributes to stress-induced anorexia and anxiety-like behavior. Endocrinology 148:5531–5540.

Livneh Y, Ramesh RN, Burgess CR, Levandowski KM, Madara JC, Fenselau H, Goldey GJ, Diaz VE, Jikomes N, Resch JM, Lowell BB, Andermann ML (2017) Homeostatic circuits selectively gate food cue responses in insular cortex. Nature 546:611–616.

Luppino FS, de Wit LM, Bouvy PF, Stijnen T, Cuijpers P, Penninx BWJH, Zitman FG (2010) Overweight, obesity, and depression. Arch Gen Psychiatry 67:220–229.

Mandelblat-Cerf Y, Ramesh RN, Burgess CR, Patella P, Yang Z, Lowell BB, Andermann ML (2015) Arcuate hypothalamic AgRP and putative POMC neurons show opposite changes in spiking across multiple timescales. Elife 4:e07122.

McDevitt DS, Graziane NM (2019) Timing of morphine administration differentially alters paraventricular thalamic neuron activity. eNeuro 6: ENEURO.0377-19.2019.

McGinty JF, Otis JM (2020) Heterogeneity in the paraventricular thalamus: the traffic light of motivated behaviors. Front Behav Neurosci 14:590528.

McNally GP (2021) Motivational competition and the paraventricular thalamus. Neurosci Biobehav Rev 125:193–207.

Meffre J, Sicre M, Diarra M, Marchessaux F, Paleressompoulle D, Ambroggi F (2019) Orexin in the posterior paraventricular thalamus mediates hunger-related signals in the nucleus accumbens core. Curr Biol 29:3298–3306.e4.

Otis JM, Zhu MH, Namboodiri VMK, Cook CA, Kosyk O, Matan AM, Ying R, Hashikawa Y, Hashikawa K, Trujillo-Pisanty I, Guo J, Ung RL, Rodriguez-Romaguera J, Anton ES, Stuber GD (2019) Paraventricular thalamus projection neurons integrate cortical and hypothalamic signals for cue-reward processing. Neuron 103:423–431.e4.

Padilla SL, Qiu J, Soden ME, Sanz E, Nestor CC, Barker FD, Quintana A, Zweifel LS, Rønnekleiv OK, Kelly MJ, Palmiter RD (2016) Agouti-related peptide neural circuits mediate adaptive behaviors in the starved state. Nat Neurosci 19:734–741.

Penzo MA, Gao C (2021) The paraventricular nucleus of the thalamus: an integrative node underlying homeostatic behavior. Trends Neurosci 44:538–549.

Penzo MA, Robert V, Tucciarone J, De Bundel D, Wang M, Van Aelst L, Darvas M, Parada LF, Palmiter RD, He M, Huang ZJ, Li B (2015) The paraventricular thalamus controls a central amygdala fear circuit. Nature 519:455–459.

Pliota P, Böhm V, Grössl F, Griessner J, Valenti O, Kraitsy K, Kaczanowska J, Pasieka M, Lendl T, Deussing JM, Haubensak W (2020) Stress peptides sensitize fear circuitry to promote passive coping. Mol Psychiatry 25:428–441.

Possa-Paranhos I, Catalbas K, Butts J, O'Berry K, Sweeney P (2023) Establishment of restraint stress–induced anorexia and social isolation–induced anorexia mouse models. Bio Protoc 13:e4597.

Qu N, He Y, Wang C, Xu P, Yang Y, Cai X, Liu H, Yu K, Pei Z, Hyseni I, Sun Z, Fukuda M, Li Y, Tian Q, Xu Y (2020) A POMC-originated circuit regulates stress-induced hypophagia, depression, and anhedonia. Mol Psychiatry 25:1006–1021.

Shah BP, Vong L, Olson DP, Koda S, Krashes MJ, Ye C, Yang Z, Fuller PM, Elmquist JK, Lowell BB (2014) *MC4R*-expressing glutamatergic neurons in the paraventricular hypothalamus regulate feeding and are synaptically connected to the parabrachial nucleus. Proc Natl Acad Sci U S A 111:13193–13198.

Sofia Beas B, Gu X, Leng Y, Koita O, Rodriguez-Gonzalez S, Kindel M, Matikainen-Ankney BA, Larsen RS, Kravitz AV, Hoon MA, Penzo MA (2020) A ventrolateral medulla-midline thalamic circuit for hypoglycemic feeding. Nat Commun 11:6218.

Sternson SM, Atasoy D (2014) Agouti-related protein neuron circuits that regulate appetite. Neuroendocrinology 100:95–102.

Su Z, Alhadeff AL, Betley JN (2017) Nutritive, post-ingestive signals are the primary regulators of AgRP neuron activity. Cell Rep 21:2724–2736.

Sutton AK, Krashes MJ (2020) Integrating hunger with rival motivations. Trends Endocrinol Metab 31:495–507.

Sweeney P, Yang Y (2015) An excitatory ventral hippocampus to lateral septum circuit that suppresses feeding. Nat Commun 6:10188.

Sweeney P, Yang Y (2017) Neural circuit mechanisms underlying emotional regulation of homeostatic feeding. Trends Endocrinol Metab 28:437–448.

Sweeney P, Chen C, Rajapakse I, Cone RD (2021a) Network dynamics of hypothalamic feeding neurons. Proc Natl Acad Sci USA 118:e2011140118.

Sweeney P, Bedenbaugh MN, Maldonado J, Pan P, Fowler K, Williams SY, Gimenez LE, Langroudi MG, Downing G, Gui Y, Hadley CK, Joy ST, Mapp AK, Simerly RB, Cone RD (2021b) The melanocortin-3 receptor is a pharmacological target for the regulation of anorexia. Sci Transl Med 13:abd6434.

Takahashi KA, Cone RD (2005) Fasting induces a large, leptin-dependent increase in the intrinsic action potential frequency of orexigenic arcuate nucleus neuropeptide Y/Agouti-related protein neurons. Endocrinology 146:1043–1047.

Vaisse C, Clement K, Durand E, Hercberg S, Guy-Grand B, Froguel P (2000) Melanocortin-4 receptor mutations are a frequent and heterogeneous cause of morbid obesity. J Clin Invest 106:253–262.

Wang D, He X, Zhao Z, Feng Q, Lin R, Sun Y, Ding T, Xu F, Luo M, Zhan C (2015) Whole-brain mapping of the direct inputs and axonal projections of POMC and AgRP neurons. Front Neuroanat 9:40.

Zhan C, Zhou J, Feng Q, Zhang JE, Lin S, Bao J, Wu P, Luo M (2013) Acute and long-term suppression of feeding behavior by POMC neurons in the brainstem and hypothalamus, respectively. J Neurosci 33:3624–3632.

Zhang J, Chen D, Sweeney P, Yang Y (2020) An excitatory ventromedial hypothalamus to paraventricular thalamus circuit that suppresses food intake. Nat Commun 11:6326.

Zhang X, van den Pol AN (2017) Rapid binge-like eating and body weight gain driven by zona incerta GABA neuron activation. Science 356:853–859.

Zhu C, Jiang Z, Xu Y, Cai ZL, Jiang Q, Xu Y, Xue M, Arenkiel BR, Wu Q, Shu G, Tong Q (2020) Profound and redundant functions of arcuate neurons in obesity development. Nat Metab 2:763–774.

Zhu Y, Nachtrab G, Keyes PC, Allen WE, Luo L, Chen X (2018) Dynamic salience processing in paraventricular thalamus gates associative learning. Science 362:423–429.

Zhu Y, Wienecke CFR, Nachtrab G, Chen X (2016) A thalamic input to the nucleus accumbens mediates opiate dependence. Nature 530:219–222.

Zhu Y-B, Wang Y, Hua X-X, Xu L, Liu M-Z, Zhang R, Liu P F, Li J-B, Zhang L, Mu D (2022) PBN-PVT projections modulate negative affective states in mice. Elife 11:e68372.